Electronic Supplementary Material (ESI) for Physical Chemistry Chemical Physics.
This journal is © the Owner Societies 2017

Thermal Convection in Electrochemical Cells. Boundaries with Heterogeneous Thermal Conductivity and Implications for Scanning Electrochemical Microscopy

Javor K. Novev and Richard G. Compton*

Department of Chemistry, Physical and Theoretical Chemistry Laboratory, Oxford University, South Parks Road, Oxford, OX1 3QZ, UK.

*Corresponding author. E-mail: Richard.Compton@chem.ox.ac.uk; Fax: +44 (0)1865 275 410; Tel: +44 (0)1865 275 957

Supplementary Information

I. Details on the simulations discussed in the main text and stability tests

This section provides additional information on the systems discussed in the main text in the form of plots of the temperature and velocity in the solution, in terms of both their volume-averages and 'snapshots' of their distributions.

Here, we also provide details on the stability of the observed flow patterns. As discussed in the main text, our approach consists in two steps – first, we substitute the zero-flux condition at the top wall of the cylinder with eq. (29) and obtain the stationary velocity and temperature distribution emerging in the modified problem. Then, we use other possible velocity, temperature and pressure distributions as initial conditions for the same simulation, thereby obtaining information about their stability in this system.

The numerical solution of the equations was sought numerically in COMSOL Multiphysics with a time-stepping algorithm with a variable step size. For most simulations at r_{cell} = 3 mm, the maximum step size was set to Δt_{max} = 3.5 s; the exception were the simulations performed in order to compare the stability of different flow patterns, see the Supplementary information. For the simulations at r_{cell} = 8 mm we used Δt_{max} = 1 s in order to describe adequately the more complicated temporal evolution of the velocity profiles.

1. Simulations for r_{cell} = 3 mm

1A. Solution colder than substrate at t = 0 (ΔT > 0)

Homogeneous BDD substrate.

Figure S1 and Figure S2 complement the discussion of the properties of the two types of flow observed in systems with homogeneous BDD substrates from the main text. In Figure S1 we plot the volume-average temperature distribution for the pattern with

clockwise motion in the simulated region. Figure S2 provides plots of the average solution velocity and temperature against time, as well as 'snapshots' of their distributions at t = 100 s for the anticlockwise pattern. Comparing Figure S1 and Figure S2B, one can infer that only the flow with clockwise motion in the simulated region has a noticeable, albeit small effect on the overall heat transfer in the solution, bringing about a change of ~1% in ΔT_{av}. The different extent of the influence of the two convective flow patterns is further illustrated by the comparison between 'snapshots' of the respective temperature profiles in Figure 2C and Figure S2D – in the latter, T is approximately independent of r, as it would be in the conduction-only case.

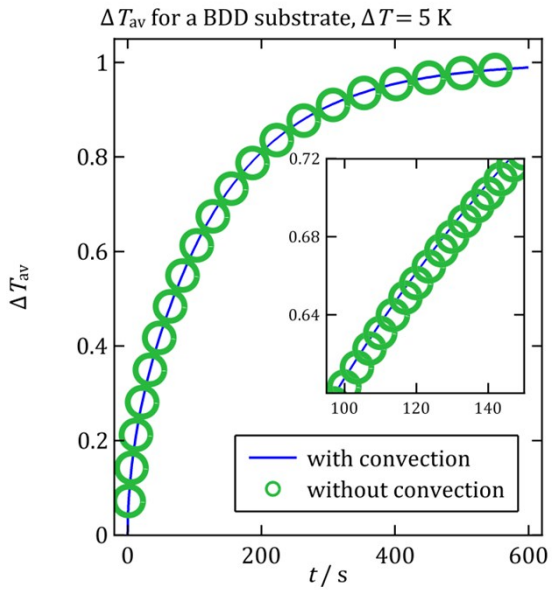

Figure S1. ΔT_{av} vs t for a homogeneous BDD substrate for the flow pattern with upwelling at r = 0 (obtained by using linear elements for T). As the inset illustrates, convection has an effect on the average temperature in the solution, although this reaches ~1 % of ΔT_{av} at most.

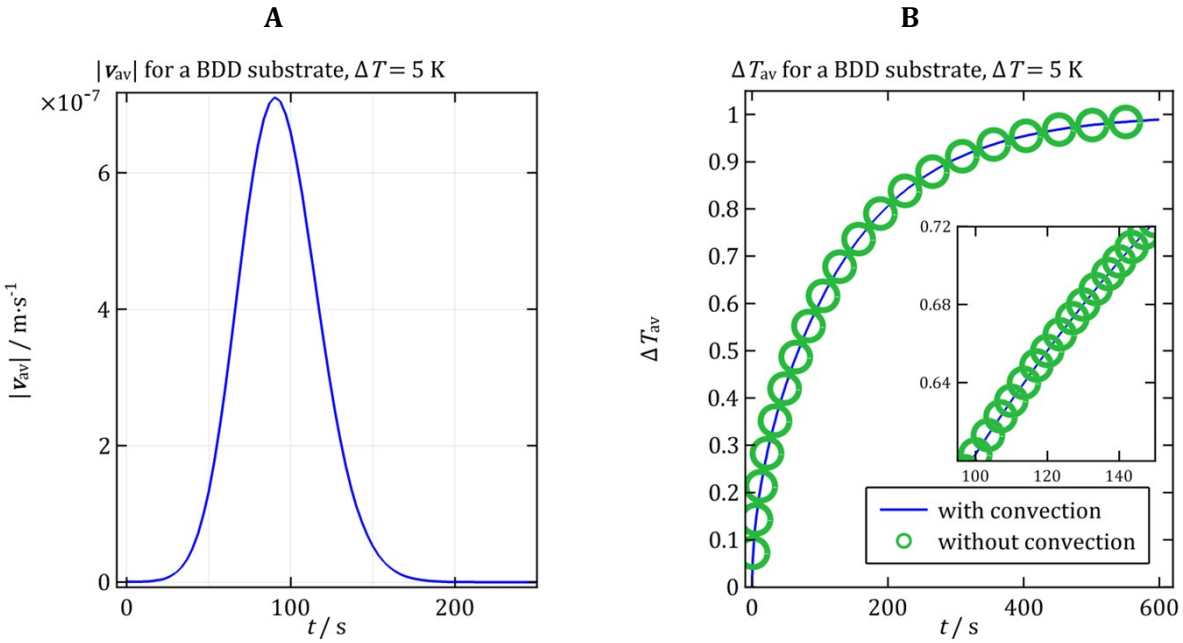

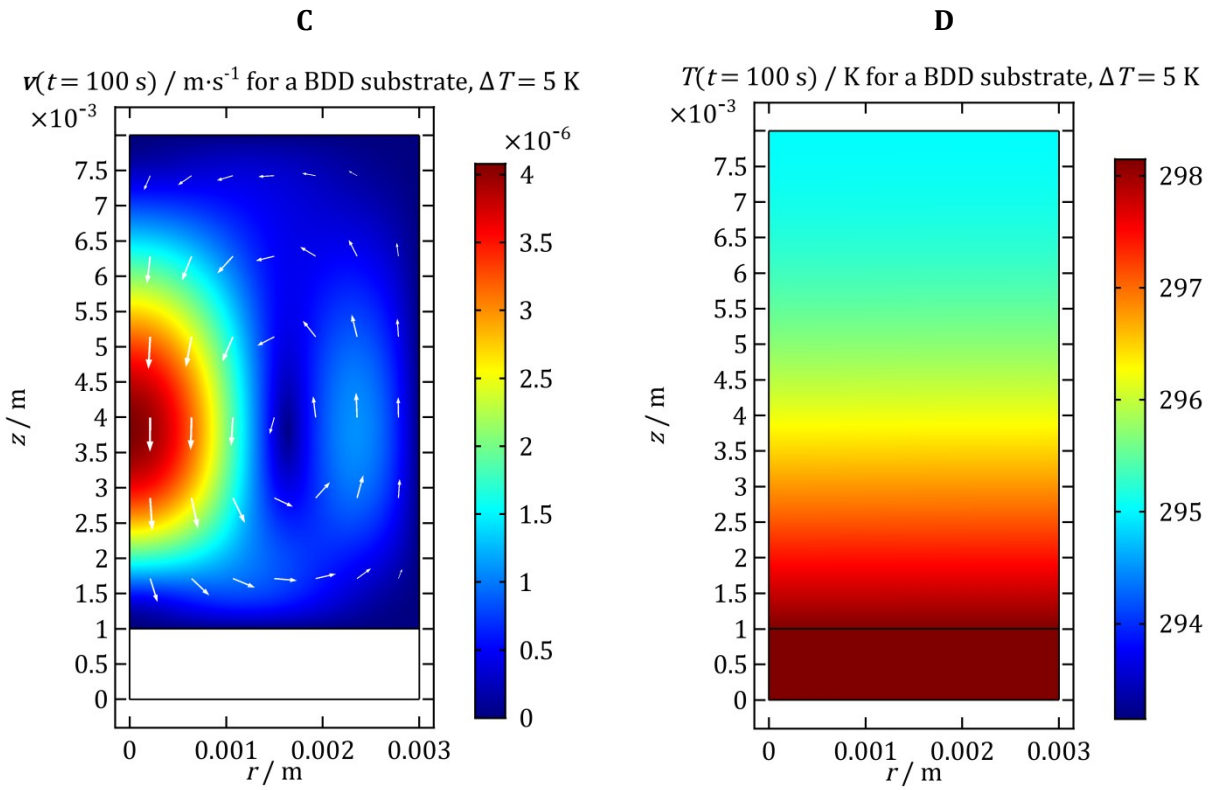

Figure S2. Results for a homogeneous BDD substrate obtained from a simulation that uses quadratic elements for T: **A** - volume-averaged velocity magnitude vs. time; **B** - volume-averaged dimensionless temperature difference; **C** and **D** -'snapshots' of $\boldsymbol{v}$ and T at t = 100 s, respectively. Note that the fluid moves downward at r = 0 in this case, in contrast with the flow pattern illustrated in Figure 2 and Figure S1.

Stability tests

Cells having a fixed-temperature top wall rather than an insulated one were simulated using both linear and quadratic shape functions for temperature. The simulations were performed in two runs for each setting – in the first run, the maximum step was set to Δt_{max} = 5 s; in the second one, the maximum step was unrestricted. For the simulation using first-order shape functions, the first run was for $t \in$ [0 s, 160 s] and the second for $t \in$ [120 s, 300 s], whereas for the simulation using second-order shape functions, the runs were for $t \in$ [0 s, 180 s] and $t \in$ [165 s, 300 s].

The results for the volume-averaged velocity magnitude are plotted versus time in Figure S3A and Figure S4A for the two types of simulations. As the figures illustrate, the simulations for long and short times yield identical results for the period of overlap. In both cases, the obtained flow patterns are qualitatively identical to those for a thermally insulated cell – compare the snapshots of $\boldsymbol{v}$ in Figure S3 and Figure S4 with these in Figure 2 and Figure S2, respectively. Notably, the plateau values of $|\boldsymbol{v}_{av}|$ are nearly identical for the two types of flow – 1.127 and 1.129x10^{-4} m·s^{-1} for the clockwise and anticlockwise, respectively; the corresponding temperature distributions are both strongly affected by convection. However, as we see in Figure S3A and Figure S4A, the flow pattern with upwelling at r = 0 reaches a stationary state quicker. Therefore, we can tentatively conclude that the faster development of one the two flows causes the difference of two orders of magnitude in intensity between them for a cell with

insulated walls (Figure 2A vs. Figure S2). The slower development of the flow with upwelling next to the side walls for the latter system means that by the time the flow pattern is established, the driving force for convection has already diminished significantly, hence the low velocity.

A further indication of the equal stability of the two flows is the fact that upon reverting from eq. (29) back to a no-flux boundary condition, the convective rolls illustrated in Figure S3-Figure S4 maintain their direction before reaching a quiescent state.

A

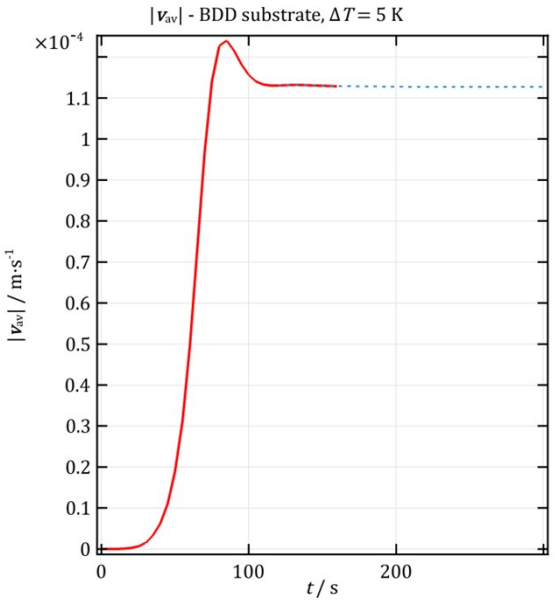

B

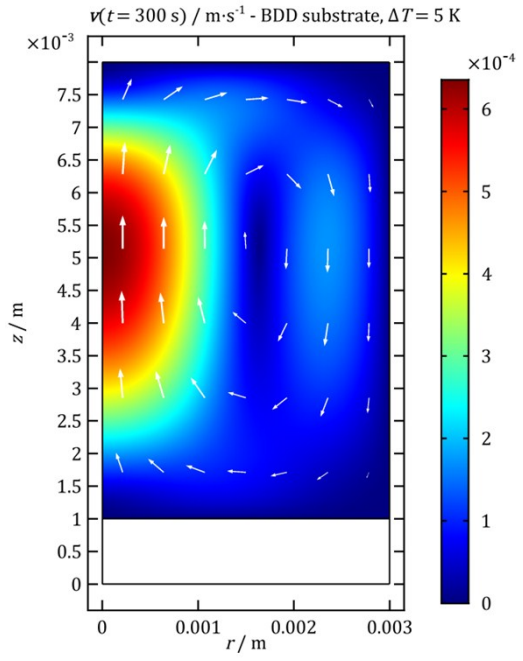

C

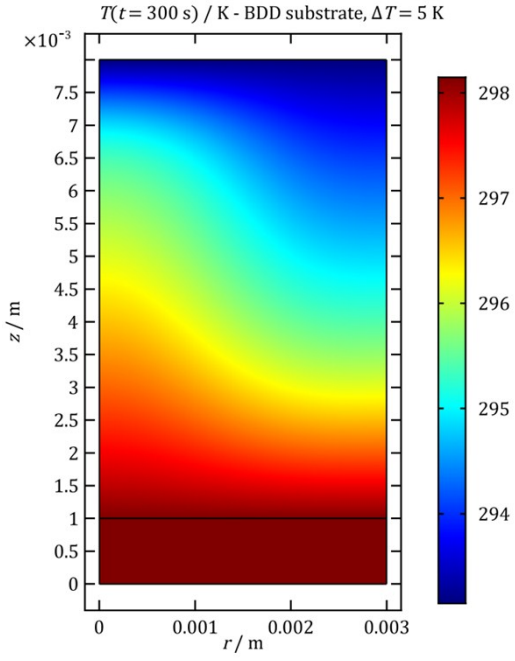

Figure S3. Results for a simulation with a fixed temperature difference between the top and bottom cell walls. The substrate is made of BDD and linear elements are used for T. **A** – volume-averaged velocity magnitude. Solid line – simulation for short t (0-160 s), dashed line – simulation for long t (120-300 s). **B** – velocity distribution at t = 300 s, **C** – temperature distribution at t = 300 s.

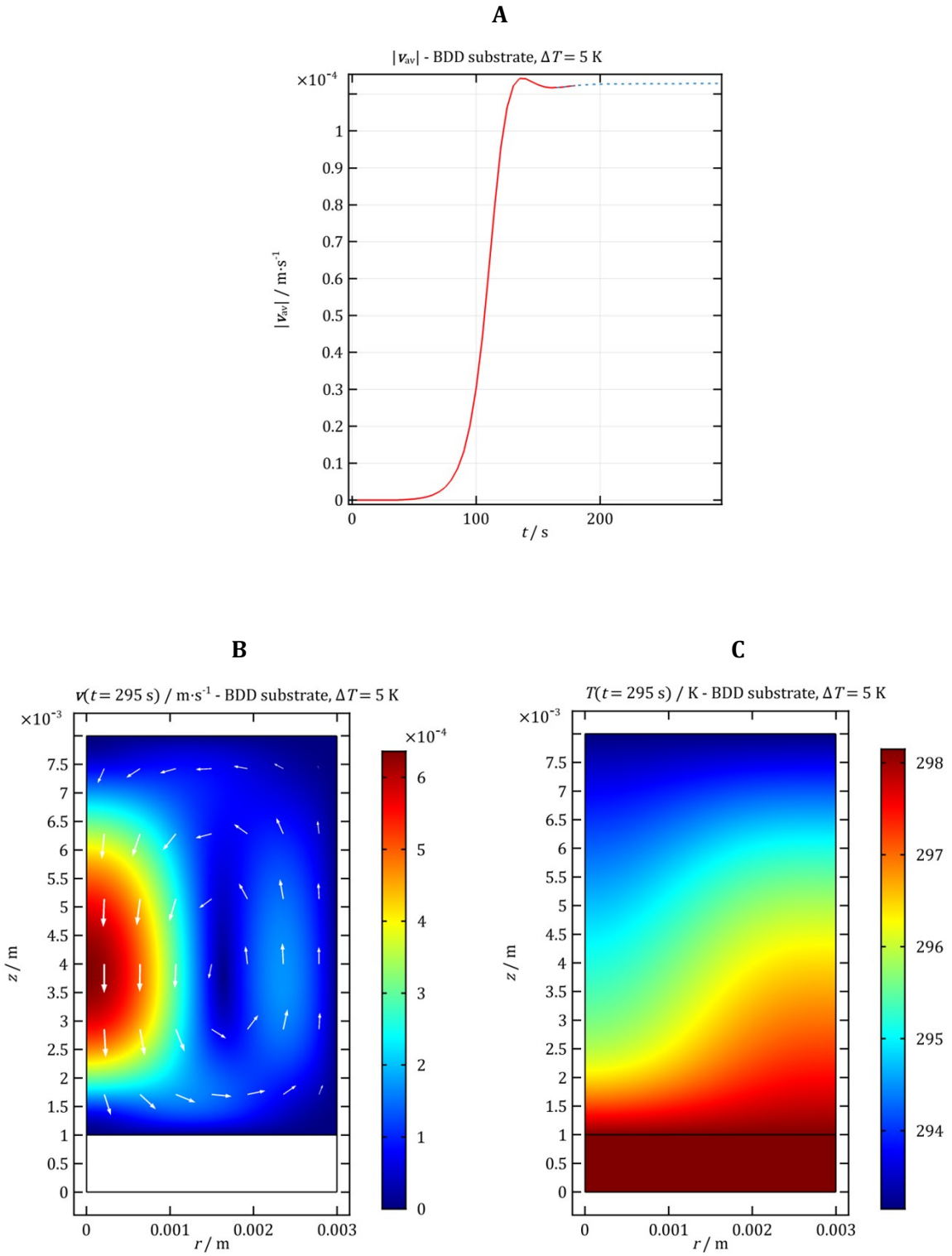

Figure S4. Results for a simulation with a fixed temperature difference between the horizontal cell walls, The substrate is made of BDD and quadratic elements are used for T. **A** – volume-averaged velocity magnitude. Solid line – simulation for short t (0-180 s), dashed line – simulation for long t (165-300 s). **B** – velocity distribution at t = 295 s, **C** – temperature distribution at t = 295 s.

A simulation employing quadratic polynomials for T was run with the stationary distributions of T, $\boldsymbol{v}$ and p (at t_0 = 300 s) from the simulation using linear elements as initial conditions and vice versa (with t_0 = 295 s); the maximum time step was Δt_{max} = 5 s for both cases. In both cases, the flow and temperature patterns from the initial condition remain unchanged throughout the simulated experiment. The average velocity relaxes from the initial condition to a stationary state within a time frame of ~30 s, as seen in Figure S5A-B. Importantly, the simulations yield the same value of $|\boldsymbol{v}_{av}|$ as the one obtained for a stagnant fluid at t = 0, the only difference being the direction of flow. This suggests that the two stationary patterns are simply mirror images of each other and that the asymmetry between Figure S3 and Figure S4 is due to the different accuracy of the simulations employing linear and quadratic shape functions.

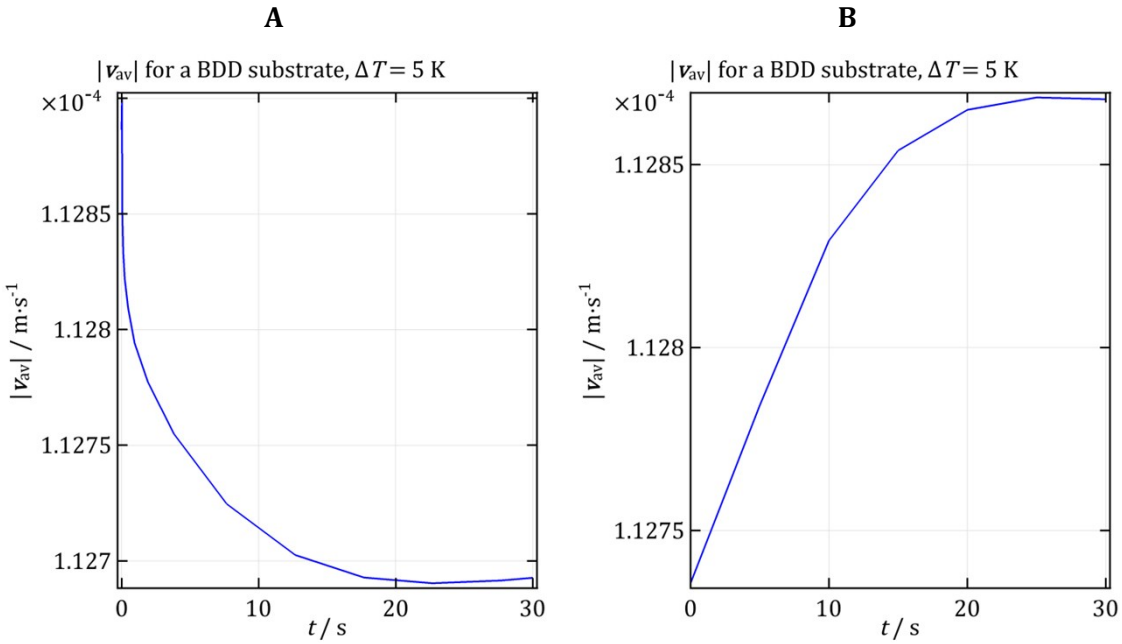

Figure S5. $|\boldsymbol{v}_{av}(t)|$ for a system with a BDD substrate and a fixed temperature difference between the top and bottom walls: **A** – linear elements for T, initial condition for anticlockwise flow in the simulated region; **B** – quadratic elements for T, initial condition for clockwise flow.

Homogeneous teflon substrate.

In this case, the velocity of the convective flows induced in the solution is negligible ($|\boldsymbol{v}_{av}| \lesssim 10^{-8}$ m·s^{-1}), and our discretization of the governing equations is no longer suitable for its description, which causes the velocity distributions exhibit high levels of numerical noise. Such low-intensity flows do not have a discernible influence on the temperature profile and would not contribute to mass transport; therefore we will not attempt to study their stability or find settings for the discretization that resolve them better. It is nonetheless worthy of note that, as with the homogeneous BDD substrate, employing linear and quadratic shape functions for T gives rise to two types of flow that differ in their direction and intensity (compare Figure S6A and Figure S7A). However, due to the low thermal conductivity of the substrate, the heat flux through its lower surface is not sufficiently intense to induce a strong perturbation in the solution density and a strong convective flow. For that reason, the overall heat transfer is essentially

unperturbed by the flow, as demonstrated by the plots of ΔT_{av} in Figure S6C-Figure S7C, and the temperature profile is approximately independent of r, as it would be in the absence of convection (Figure S6C-Figure S7C).

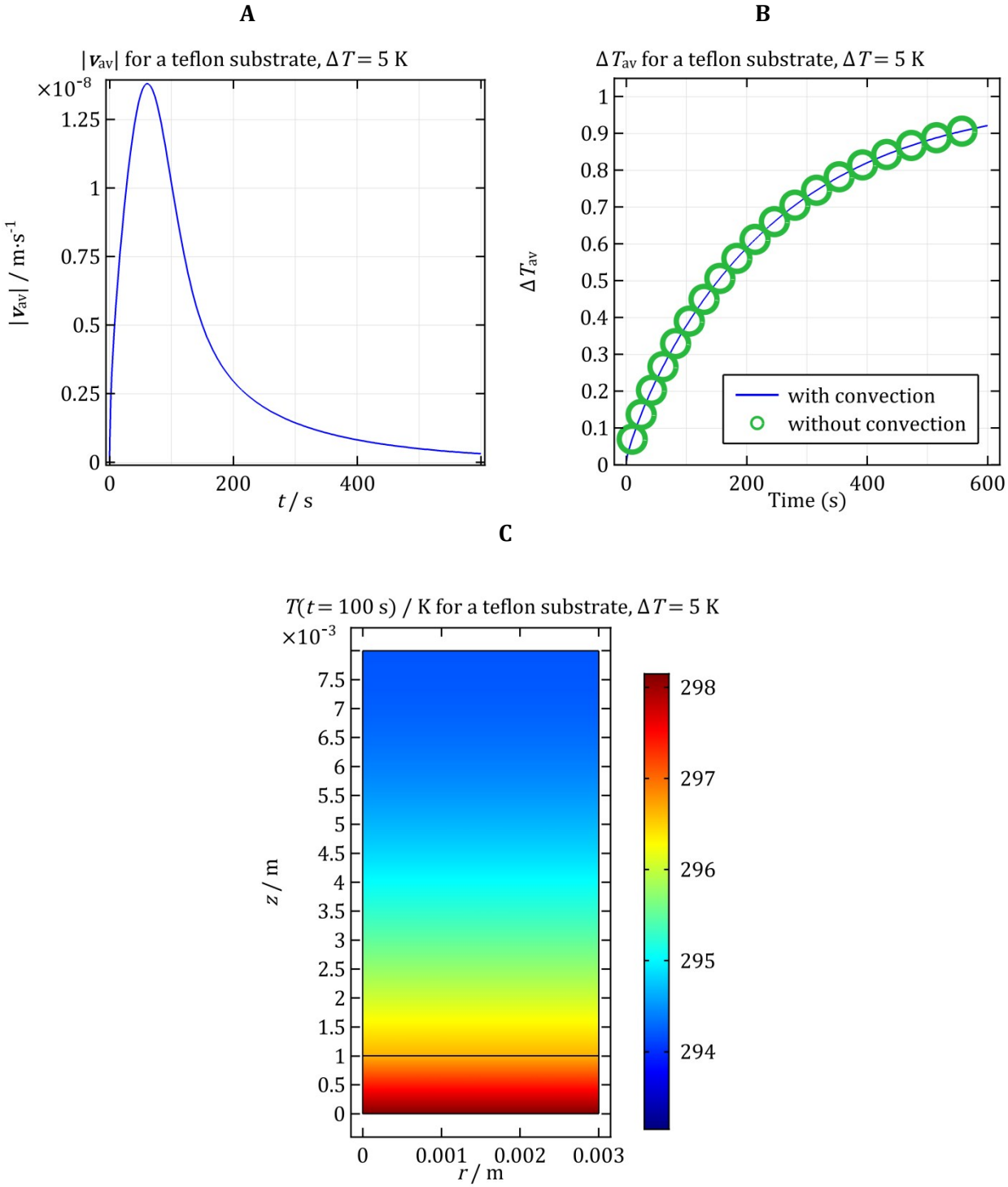

Figure S6. Results for a cell with a homogeneous teflon substrate at its bottom, simulated using linear elements for T. **A** – volume-averaged velocity, $|v_{av}(t)|$; **B** – volume-averaged dimensionless temperature difference, ΔT_{av}; **C** – temperature distribution at t = 100 s.

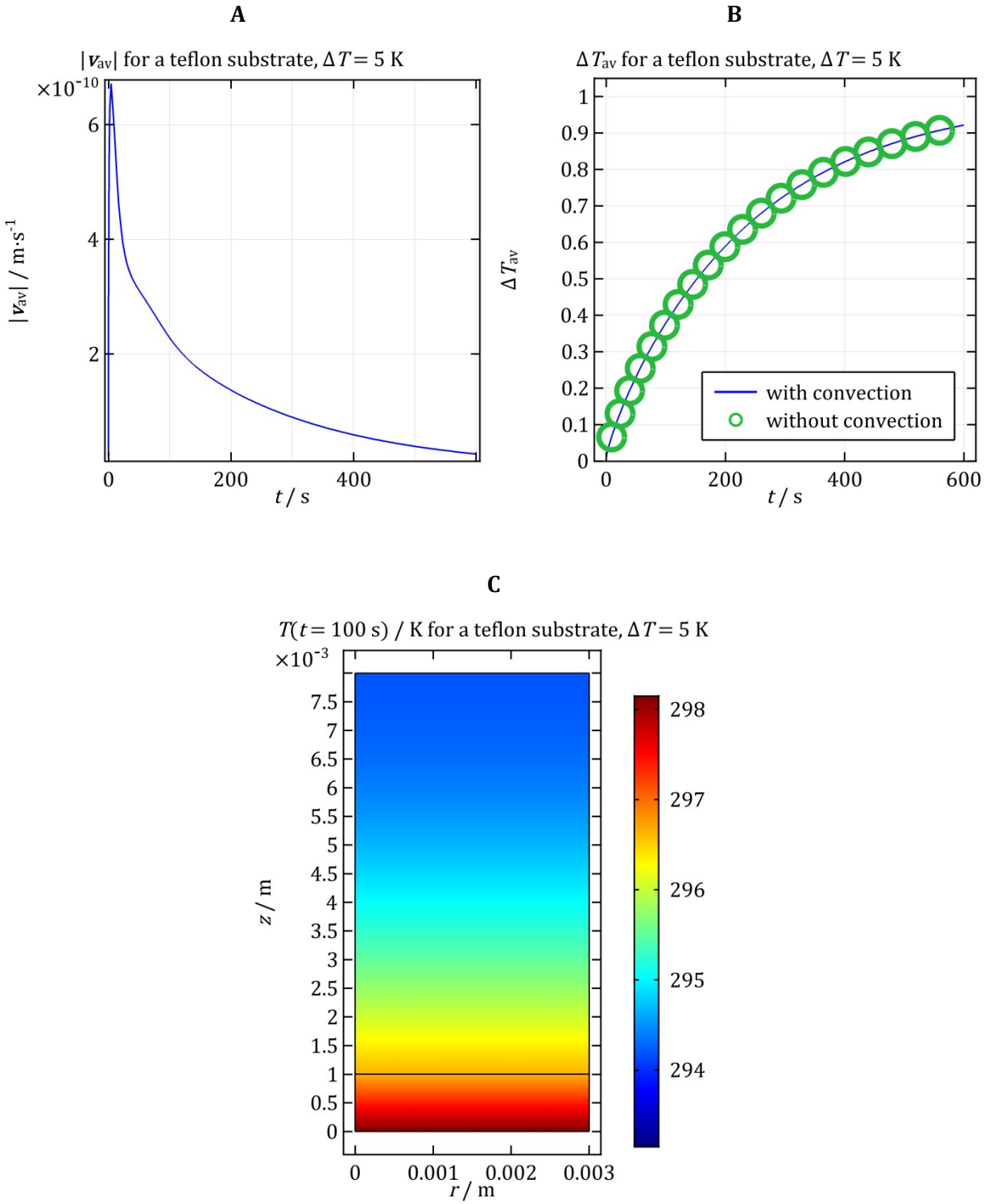

Figure S7. Results for a cell with a homogeneous teflon substrate at its bottom, simulated using quadratic elements for T. **A** – volume-averaged velocity, $|\boldsymbol{v}_{av}(t)|$; **B** – volume-averaged dimensionless temperature difference, ΔT_{av}; **C** – temperature distribution at t = 100 s.

BDD substrates with teflon annular bands

In Figure S8, we provide 'snapshots' of the velocity and temperature distributions for this configuration at the approximate moment in time when the average solution velocity reaches its peak value, complementing Figure 3 from the main text.

Figure S9 and Figure S10 present the results from our studies with varying ΔT, depicting the volume-averaged dimensionless temperature difference and the volume-averaged velocity for the different substrates. As seen in Figure S9, the difference between ΔT_{av} for the simulations involving convection and the conduction-only case is nearly zero at ΔT = 3 and 4 K, whereas for ΔT = 5 K, it reaches a maximum value of 2.5, 5.8 and 7.5 % for d_{band}/r_{cell} = 1/27, 1/9 and 1/3, respectively. Figure S10 demonstrates that this qualitative difference in behaviour is brought about by a sharp increase in the average solution velocity.

For verification purposes, we ran simulations of BDD substrates with a teflon annular band employing quadratic shape functions for T, which yielded the same qualitative results as those using linear, but the maximum volume-averaged velocity was higher for the second-order polynomials, the variation being 4.2% for d_{band}/r_{cell} = 1/27, 0.3% for d_{band}/r_{cell} = 1/9 and 0.13 % for d_{band}/r_{cell} = 1/3.

A **B**

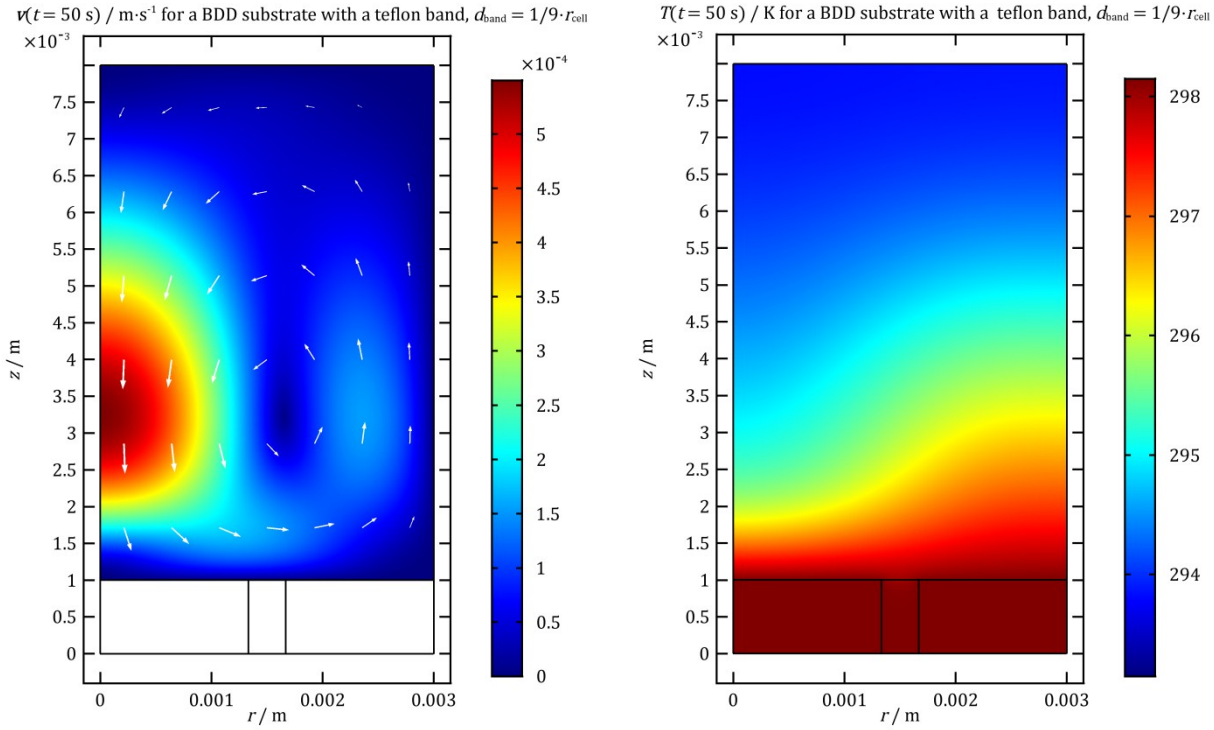

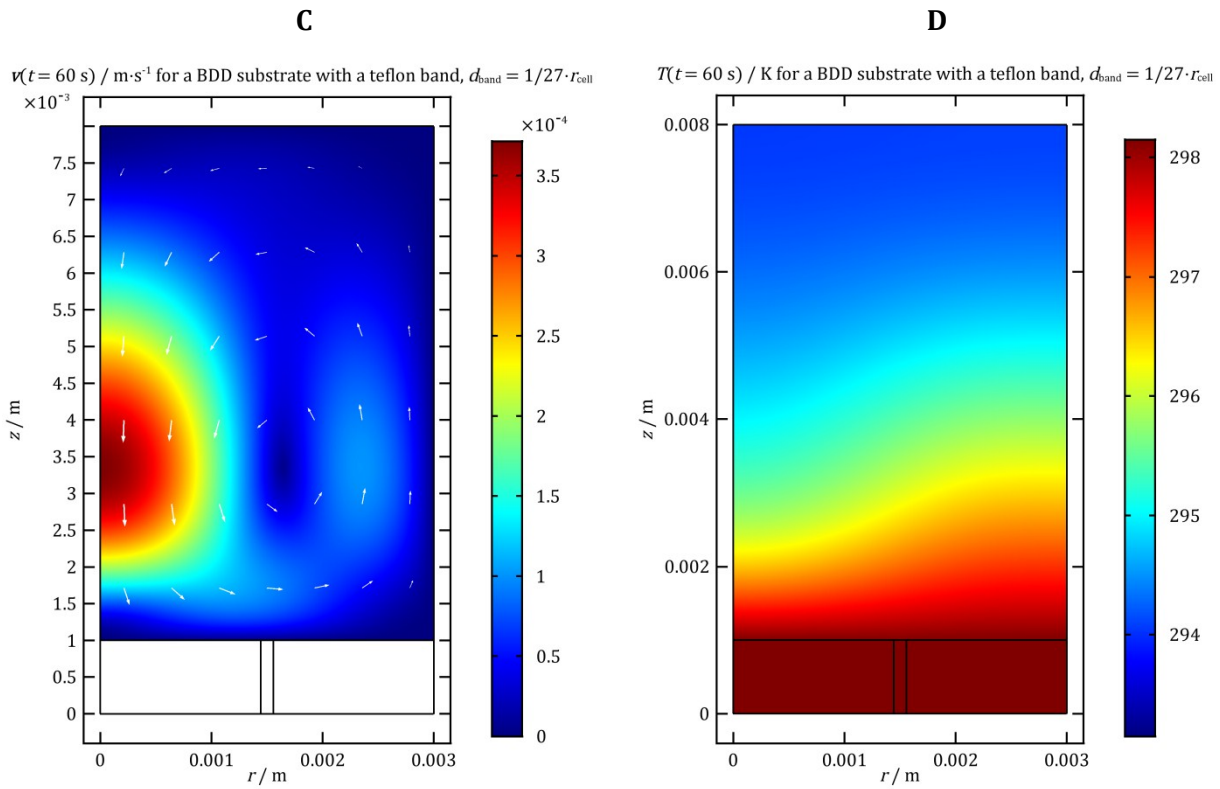

Figure S8.Results for BDD substrates with a teflon annular band. **A**, **B** – velocity and temperature profiles at t = 50 s for d_{band}/r_{cell} = 1/9; **C**, **D** – $\boldsymbol{v}(t = 60\ s)$, $T(t = 60\ s)$, d_{band}/r_{cell} = 1/27.

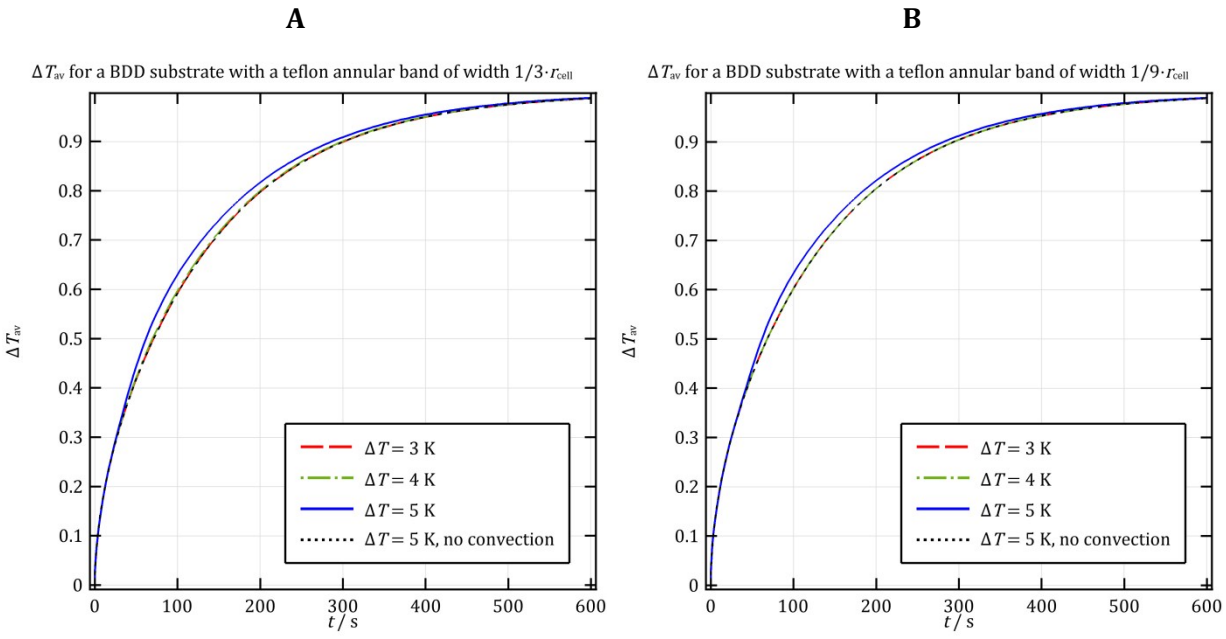

C

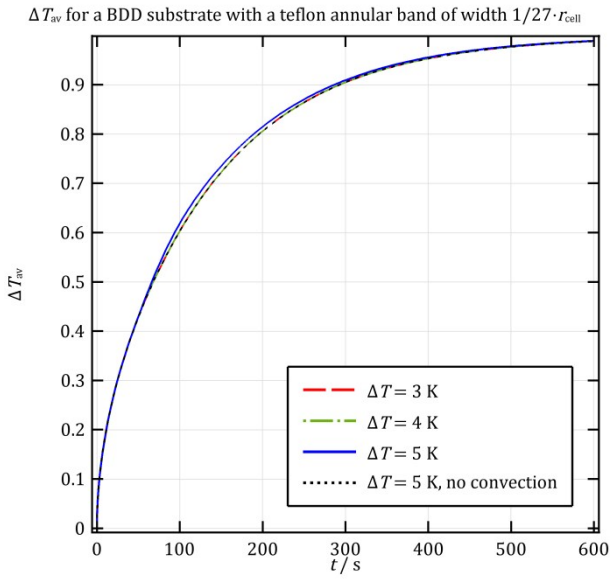

Figure S9. $\Delta T_{av}(t)$ for BDD substrates with teflon annular bands of varying width, d_{band} equal to **A** – $r_{cell}/3$, **B** – $r_{cell}/9$, **C** – $r_{cell}/27$.

A

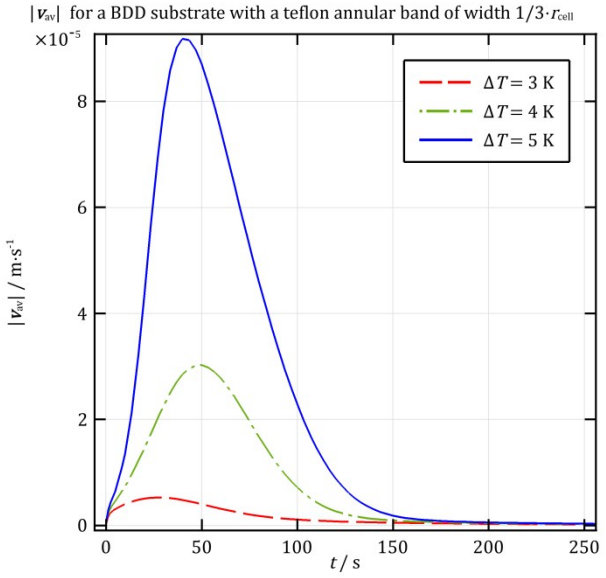

B

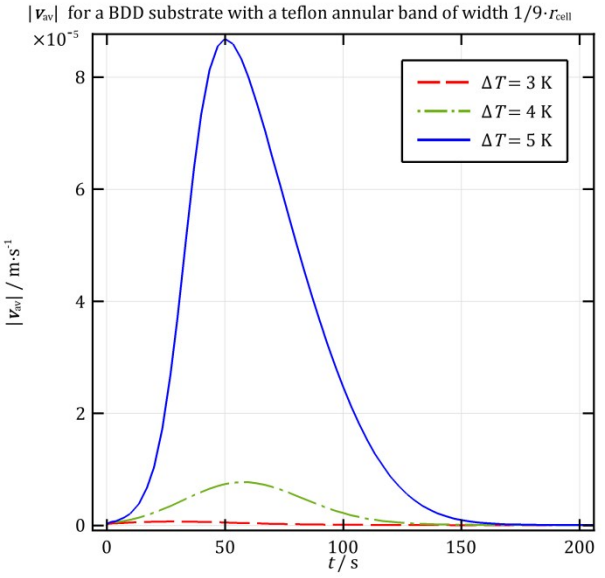

C

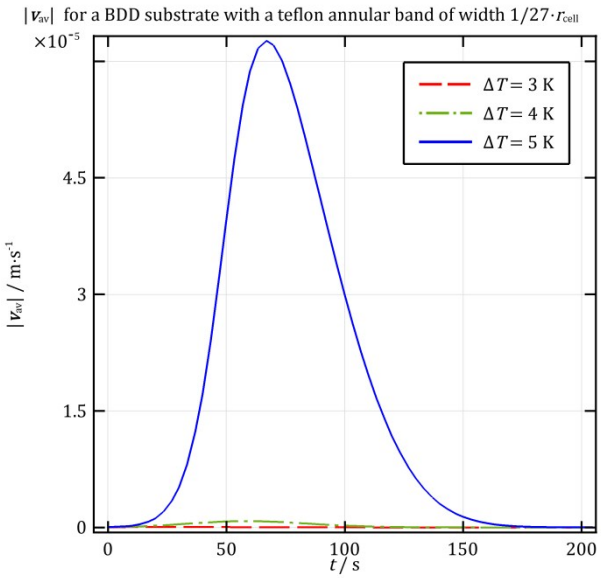

Figure S10 $|\boldsymbol{v}_{av}(t)|$ for BDD substrates with teflon annular bands of varying width, d_{band} equal to **A** – $r_{cell}/3$, **B** – $r_{cell}/9$, **C** – $r_{cell}/27$.

Stability tests

We also performed a qualitative stability analysis of the flows observed for BDD substrates with teflon annular bands. To do this, we substituted the no-flux boundary condition at the top wall with eq. (29), as we did for homogeneous BDD substrates. The simulations were performed in two stages, the first having a maximum time step of 3.5 s, covering the period $t \in [0\text{ s}, 115\text{ s}]$. The second stage had an unrestricted maximum time step and was for the interval $[t_{in}, 300\text{ s}]$, where $t_{in} = 90.9$ s, 89.8 s and 93.3 s for $d_{band}/r_{cell} = 1/3$, $1/9$ and $1/27$, respectively. As the plot of $|\boldsymbol{v}_{av}(t)|$ in Figure S11A shows, the results from the two stages are consistent with each other in the region of overlap. The flow patterns and the temperature profiles at the stationary state, shown in Figure S11B-C for $d_{band}/r_{cell} = 1/3$, are consistent with those obtained for a cell with thermally insulated walls in that the fluid moves downwards at the cylinder axis, compare with Figure 3.

We tested the stability of the observed flow pattern with upwelling at the side wall of the cylinder qualitatively by taking $\boldsymbol{v}$, T and p at the stationary state at $t \approx 300$ s as initial conditions, and reverting to a no-flux boundary condition at the top wall. This had no qualitative effect on the flow pattern apart from leading to a gradual decay and the eventual establishment of a quiescent equilibrium state, as in our other simulations of cells with thermally insulated walls.

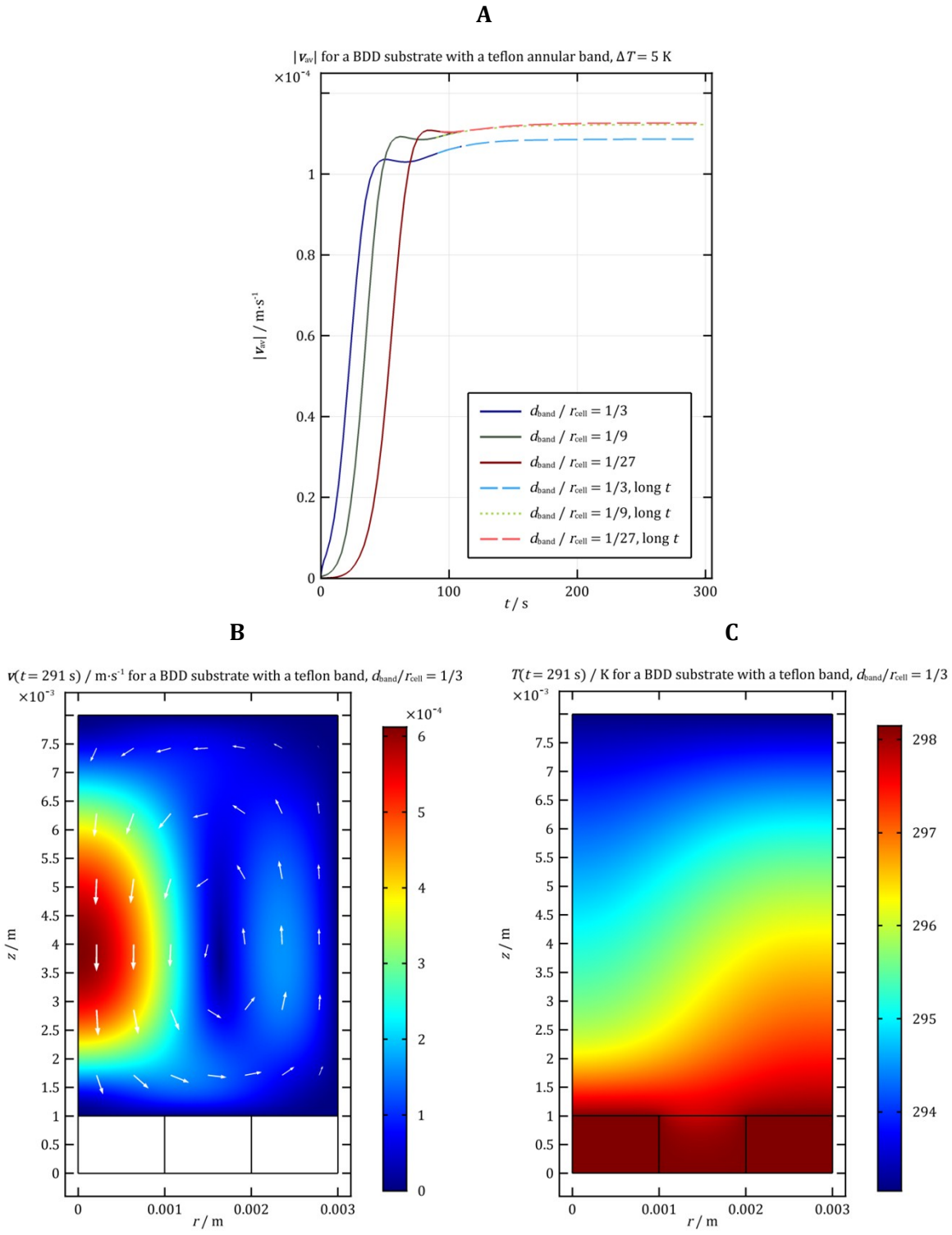

Figure S11. Results for simulations with a fixed temperature difference between the top and bottom cell walls, The substrate is made of BDD and has a teflon annular band. **A** – volume-averaged velocity magnitude. Solid lines – simulations for short t, dashed/dotted lines – simulations for long t (see text for details). **B** and **C** – velocity and temperature distributions for d_{band}/r_{cell} = 1/3 at t = 291 s.

As we did for homogeneous conductive substrates, we performed additional studies of the stability of the flow pattern in which there is upwelling instead of downflow at r = 0, i.e., the approximate mirror image of the one discussed above. To do this, we took the stationary velocity profile with clockwise motion in the simulated region from the simulation of a homogeneous BDD substrate with the boundary

condition (29), as well as the stationary distributions of the pressure and the temperature of the liquid (all at $t \approx 300$ s). For T^S, we used the stationary distribution at $t \approx 300$ s for the respective d_{band} as obtained from the simulations of BDD substrates with teflon annular bands with initial conditions for stagnant solution. The simulations were run in two stages, the first one covering the temporal interval [0 s, 30 s] and having a maximum time step of 5 s. The second stage was for $t \in$ [15.39 s, 120 s], [15.658 s, 120 s] and [17.68 s, 65 s] for $d_{\text{band}}/r_{\text{cell}} = 1/3$, 1/9 and 1/27, respectively and had no restriction on the time step. The length of the simulated experiment was greater for the larger annular bands because of the longer characteristic time for attaining a stationary velocity profile (see Figure S12A). The initial velocity and temperature distributions in the liquid were preserved qualitatively, as shown in Figure S12B-C. This indicates that toroidal rolls with upwelling at $r = 0$ and $r = r_{\text{cell}}$ are approximately equivalent in stability provided that driving force for convection is constant.

A

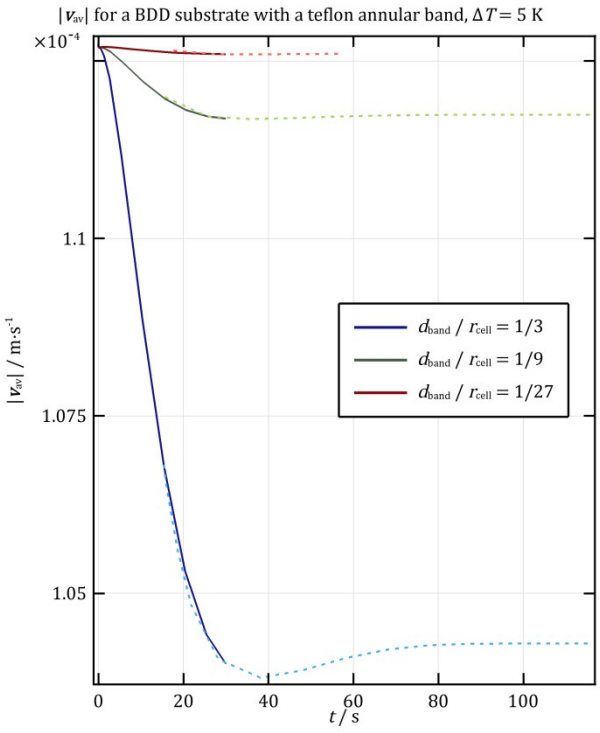

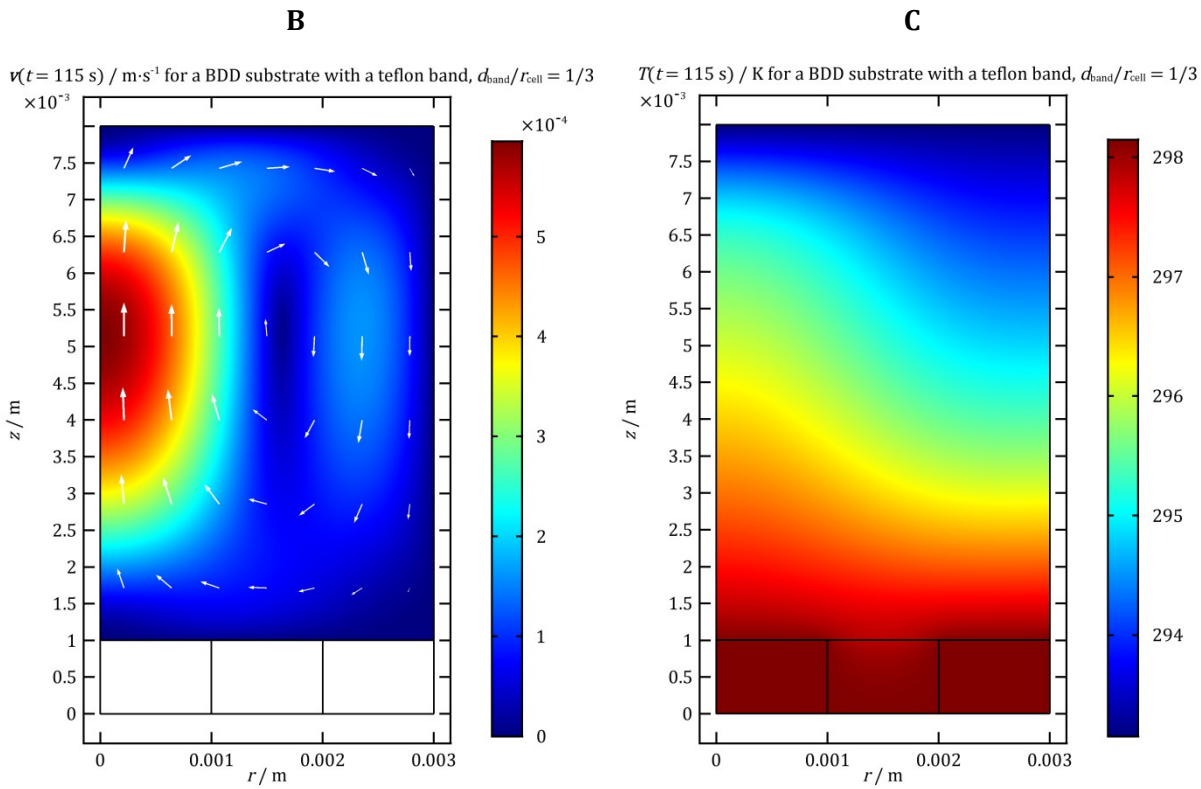

Figure S12. Results for BDD substrates with teflon annular bands from simulations with a fixed temperature difference between the top and bottom cell walls. The initial conditions for $\mathbf{v}$, T^{L} and p correspond to upwelling in the cylinder centre and are taken from the simulation of a homogeneous BDD substrate that uses linear elements for T. T^{S} is taken from the stationary prediction of the simulation of the same substrate with stagnant initial conditions. **A** – volume-averaged velocity magnitude. Solid lines – simulations for short t, dashed/dotted lines – simulations for long t (see text for details). **B** and **C** – velocity and temperature distributions for d_{band}/r_{cell} = 1/3 at t = 115 s.

As an additional test of the stability of the flow pattern with upwelling at $r = 0$, which we did not observe for simulations with stagnant initial conditions, we ran simulations with the top boundary condition changed back to no-flux and using as initial conditions the distributions of $\boldsymbol{v}$, T and p at the stationary state as predicted by the simulations illustrated in Figure S12. The flow patterns underwent complex evolution and the upwelling at $r = 0$ was not preserved. Thus, our data suggests that for BDD substrates with a teflon annular band, the roll with downward fluid motion at the cylinder axis is more stable under transient conditions than its approximate mirror image about $z = h_s$, even though the two are equivalent in stability under stationary conditions.

Teflon substrates with BDD annular bands

Figure S13 shows 'snapshots' of $\boldsymbol{v}$ and T for model cells with insulated top and side walls in contact with teflon substrates with BDD annular bands. The plots in Figure S13A-Figure S13D illustrate the velocity and temperature distribution for d_{band}/r_{cell} = 1/9 and 1/27 at a moment of time chosen to be close to the peak of $|\boldsymbol{v}_{av}(t)|$ and thus complement Figure 4B-C.

In Figure S14 and Figure S15, we present $|\boldsymbol{v}_{av}(t)|$ and $\Delta T_{av}(t)$ for d_{band}/r_{cell} = 1/9 and 1/27 at varying initial temperature differences. As in the case with d_{band}/r_{cell} = 1/3 (Figure 5 in the main text), we see a sharp increase in the convective velocity that causes

$\Delta T_{av}(t)$ to deviate significantly from the conduction-only case as ΔT is increased from 4 to 5 K. At ΔT = 5 K, the relative difference with the simulations involving no convection reaches a maximum value of 5.5%, 8.0% and 11.5% for d_{band}/r_{cell} = 1/27, 1/9 and 1/3, respectively.

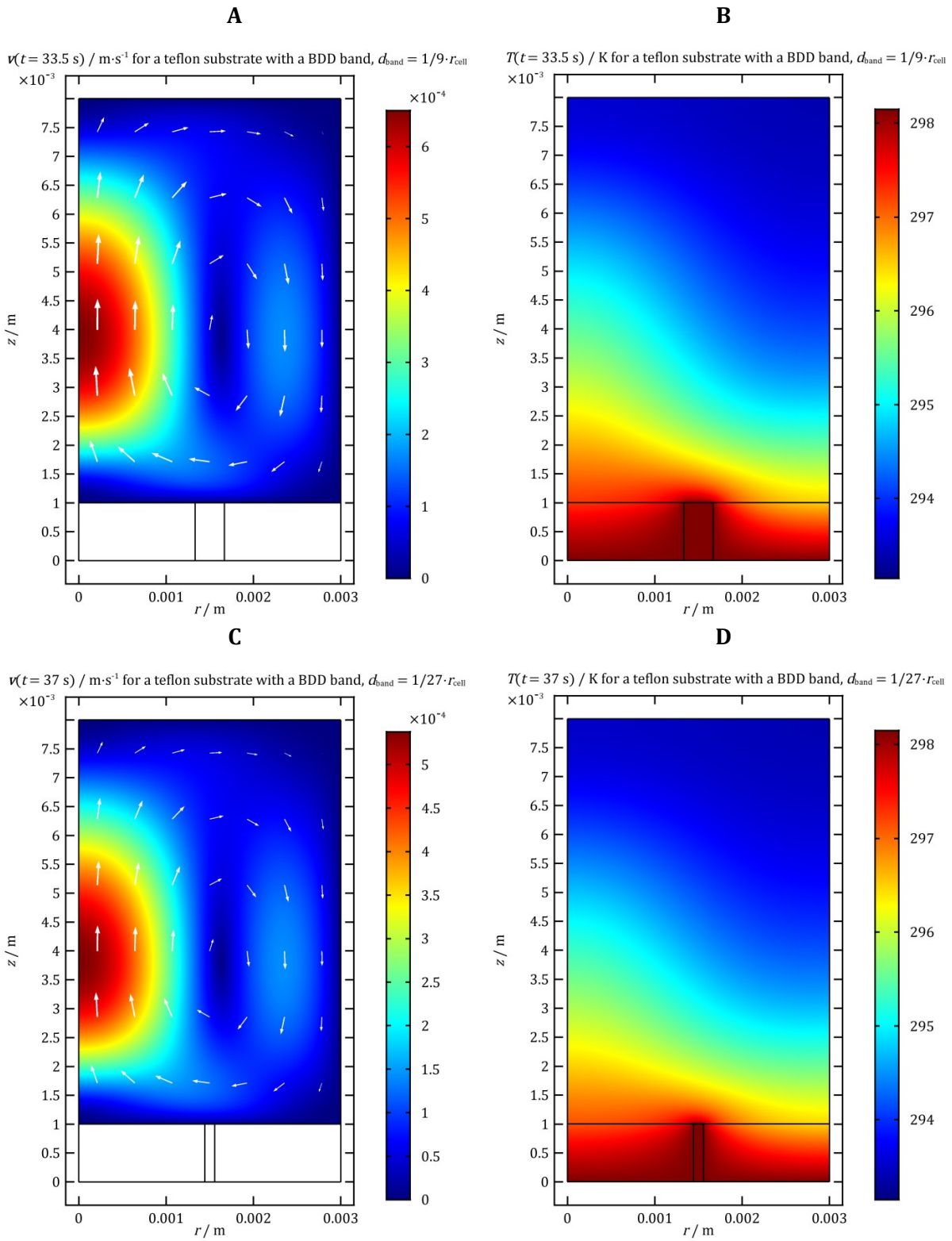

Figure S13. Results for teflon substrates with BDD annular bands. **A**, **B** – velocity and temperature profiles at t = 33.5 s for d_{band}/r_{cell} = 1/9; **C**, **D** – $\boldsymbol{v}(t$ = 37 s), $T(t$ = 37 s), d_{band}/r_{cell} = 1/27.

For verification purposes, we performed simulations employing quadratic shape functions for T, as we did for the 'inverse' configuration. We obtained identical results as we did using linear elements, again with minor differences in the numerical values, the variation in $|\boldsymbol{v}_{\mathrm{av}}|_{\max}$ being 0.5 % for $d_{\mathrm{band}}/r_{\mathrm{cell}} = 1/27$, 1.1 % for $d_{\mathrm{band}}/r_{\mathrm{cell}} = 1/9$ and 0.4 % for $d_{\mathrm{band}}/r_{\mathrm{cell}} = 1/3$.

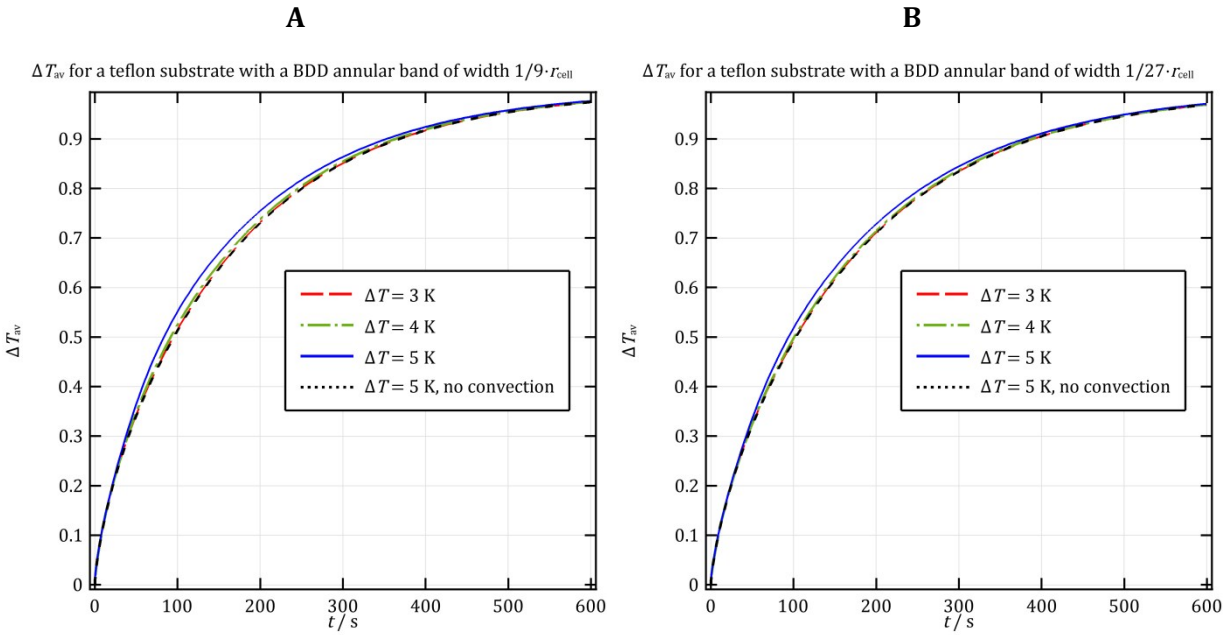

Figure S14. $\Delta T_{\mathrm{av}}(t)$ at varying initial temperature differences ΔT for teflon substrates with BDD annular bands of varying width, d_{band} equal to **A** – $r_{\mathrm{cell}}/9$, **B** – $r_{\mathrm{cell}}/27$.

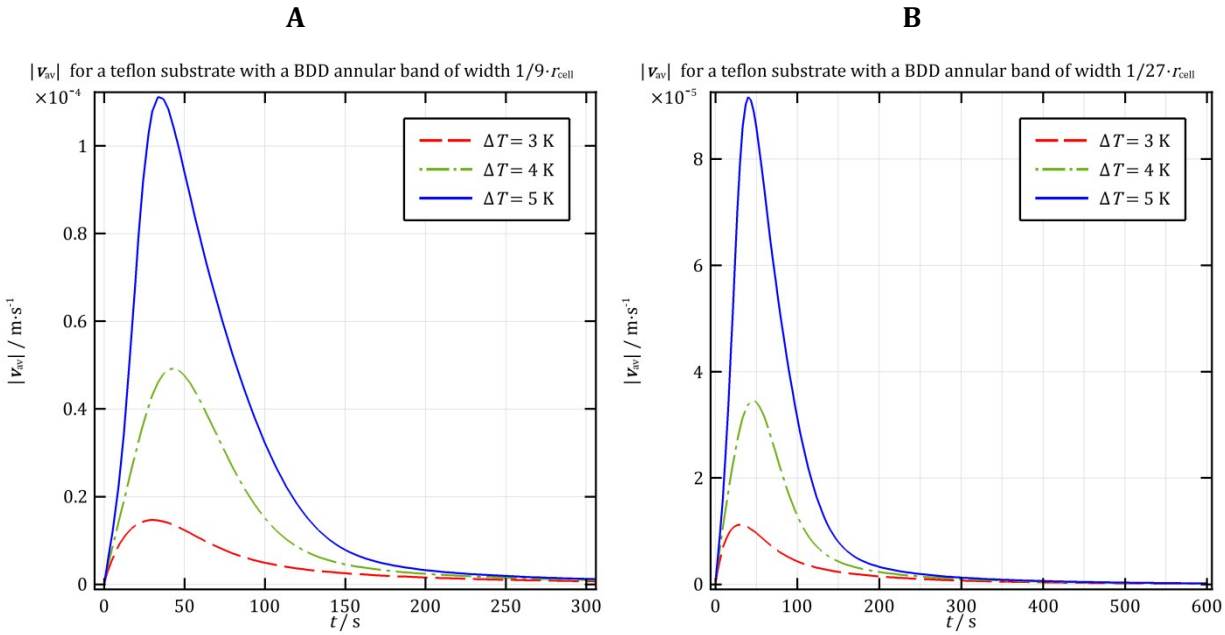

Figure S15. $|\boldsymbol{v}_{\mathrm{av}}|$ at varying initial temperature differences ΔT for teflon substrates with BDD annular bands of varying width, d_{band} equal to **A** – $r_{\mathrm{cell}}/9$, **B** – $r_{\mathrm{cell}}/27$.

Stability tests

Simulations of teflon substrates with BDD annular bands were also run with linear elements for T and the boundary condition (29) that permits a stationary state. As

in the previous cases, the simulations were run with a restriction on the maximum time step (Δt_{max} = 3.5 s) at short t and with no restriction at long t. The simulated time periods were [0 s, 100 s] for the initial stage and [t_{in}, 300 s] for the latter one, where t_{in} = 79.1 s, 78.7 s and 75.7 s for $d_{band}/r_{cell} = 1/3$, 1/9 and 1/27, respectively. Figure S16A presents the dependence of $|\boldsymbol{v}_{av}|$ on t for these cases and demonstrates that the simulations for long t agree with those for short t at the region of overlap. The stationary flow patterns and the temperature distributions, illustrated in Figure S16B-C for $d_{band}/r_{cell} = 1/3$, are qualitatively identical to those observed in the case of a cell with thermally insulated walls, seen in Figure 4B-C.

By analogy with our treatment of the 'inverse' configuration, teflon substrates with BDD annular bands, we subjected the flow patterns with upwelling at $r = 0$ to a simple stability test. For that purpose, we set the boundary condition at the top cylinder wall back to that for thermal insulation and used the profiles $\boldsymbol{v}$, T and p at the stationary state (as illustrated in Figure S16) as initial conditions. The flow diminished in intensity as the solution temperature approached its equilibrium state but its direction remained unchanged.

A

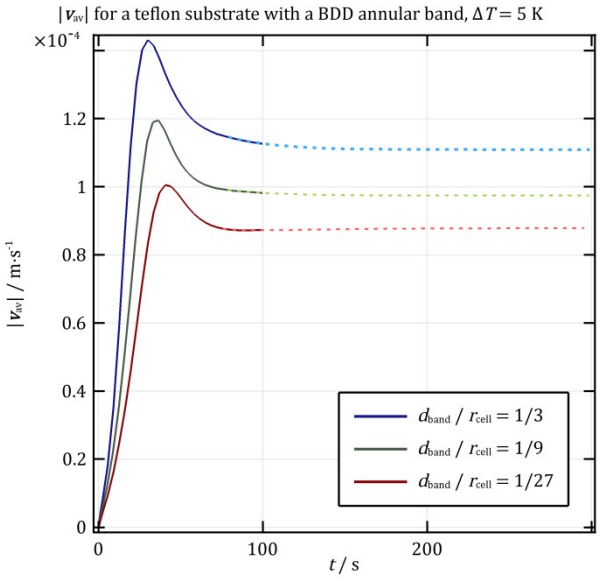

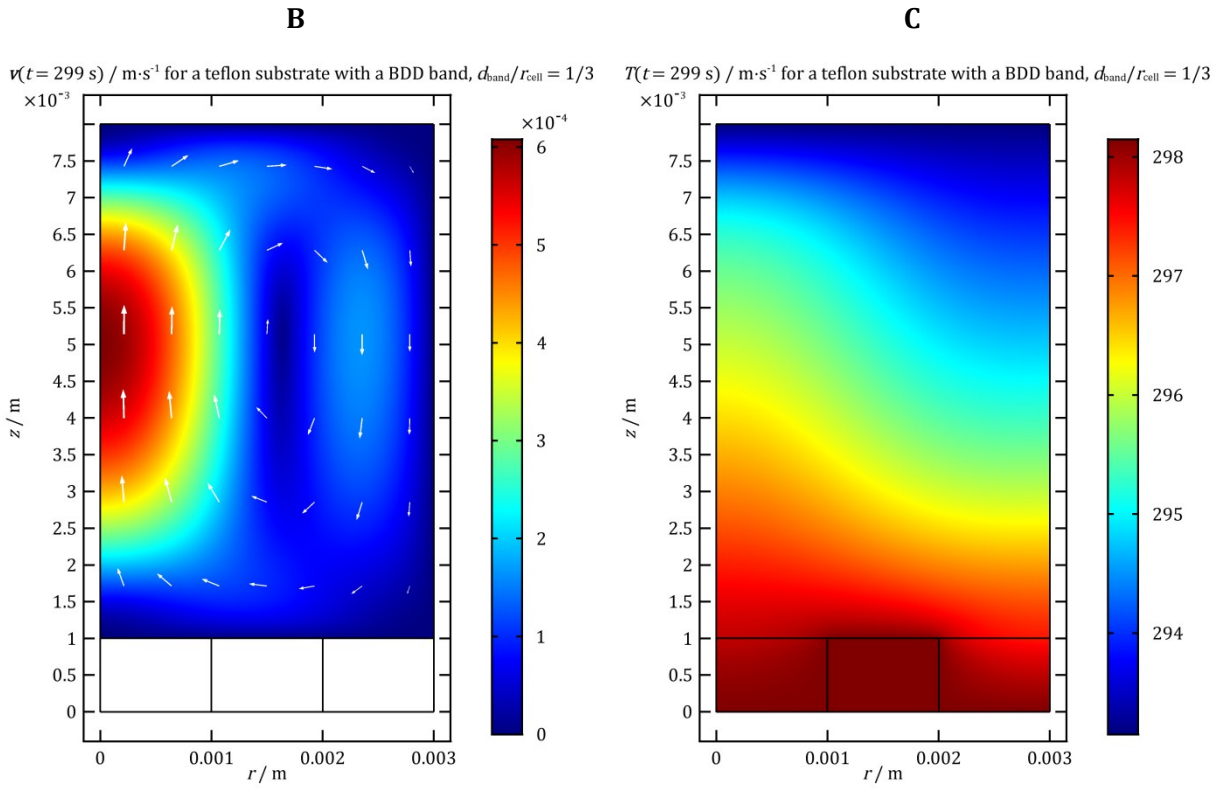

Figure S16. Results for simulations with a fixed temperature difference between the top and bottom cell walls, The substrate is made of teflon and has a BDD annular band. **A** – volume-averaged velocity magnitude. Solid lines – simulations for short t, dashed/dotted lines – simulations for long t (see text for details). **B** and **C** – velocity and temperature distributions for $d_{band}/r_{cell} = 1/3$ at $t = 299$ s.

As with the case of a homogeneous conductive substrate and a BDD substrate with a teflon annular band, we also tested whether a flow with the opposite direction would be stable. As initial conditions, we took the stationary profiles of $\boldsymbol{v}$, T and p in the liquid from a simulation of a BDD substrate that yields an anticlockwise flow in the simulated region (see Figure S4) and the stationary temperature distribution in the solid (both at $t \approx 300$ s) from the simulations of the teflon substrates with the corresponding d_{band} and initial conditions for stagnant solution (seen in Figure S16C for $d_{band} = 1/3 r_{cell}$). The simulations were run in two stages, the first one covering the interval [0 s, 100 s] with a maximum time step of 5 s. For the second stage, encompassing [80 s, 300 s], the time step was unconstrained. In all cases, the flow pattern and the shape of the temperature profile of the liquid from the initial condition were preserved. Figure S17A illustrates that the system reached a steady state in ~200 s, the time scale necessary for the temperature of the substrate to evolve from the profile in the initial condition (Figure S16C) to the stationary one for the present case (Figure S17). Thus, as in the case of the 'inverse' configuration, the rolls with upwelling and downflow at $r = 0$ are both stable under boundary conditions that permit a stationary flow.

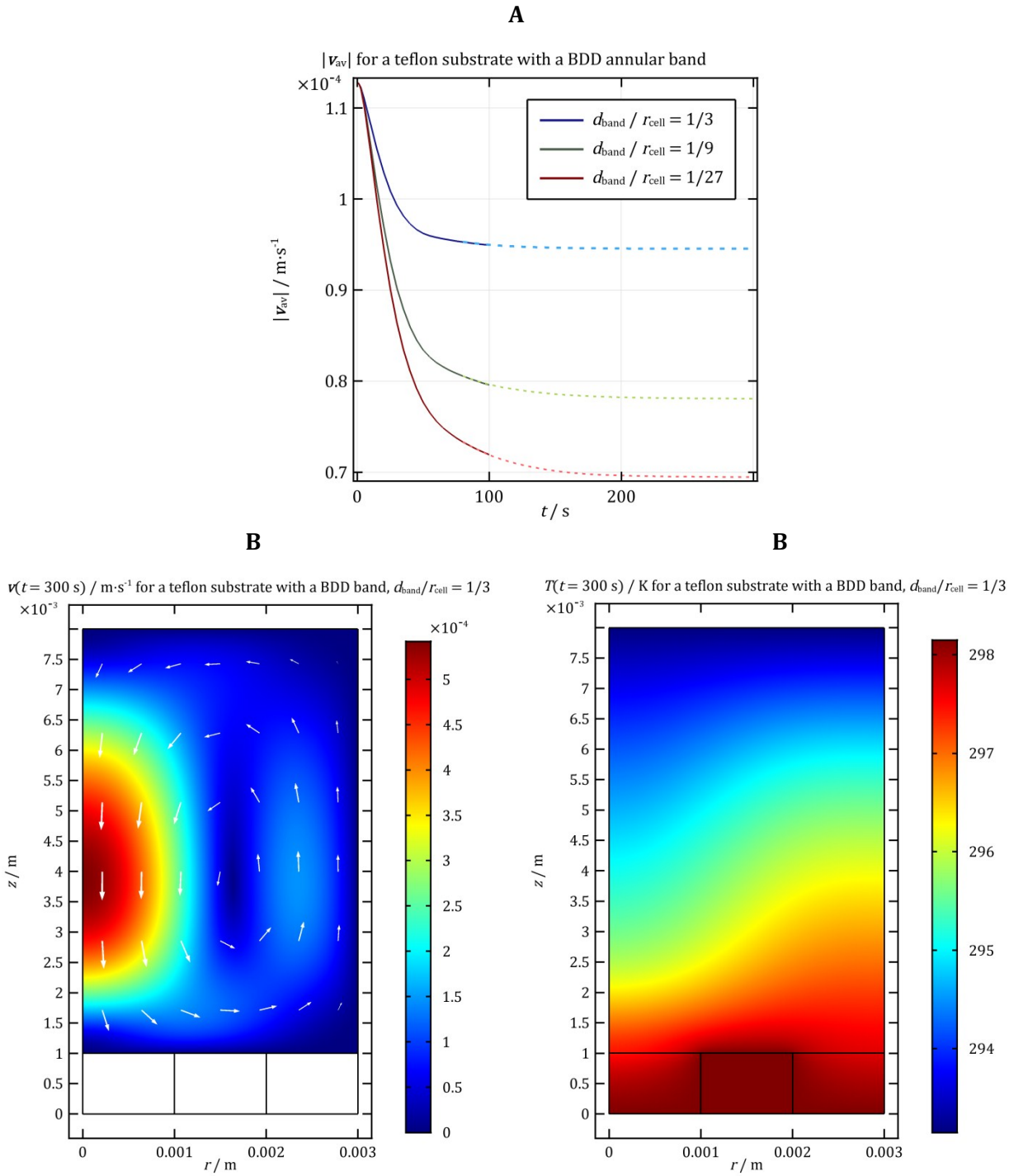

Figure S17. Results for teflon substrates with BDD annular bands from simulations with a fixed temperature difference between the top and bottom cell walls. The initial conditions for **v**, T^{L} and p correspond to upwelling at side wall of the cylinder centre and are taken from the simulation of a homogeneous BDD substrate that uses quadratic elements for T. T^{S} is taken from the stationary prediction of the simulation of a teflon substrate with a BDD annular band with the respective value of d_{band} that employs stagnant initial conditions. **A** – volume-averaged velocity magnitude. Solid lines – simulations for short t, dashed/dotted lines – simulations for long t (see text for details). **B** and **C** – velocity and temperature distributions for d_{band}/r_{cell} = 1/3 at t = 300 s.

Again by analogy with the case of BDD substrates with teflon annular bands, we also changed the boundary condition back to that for a cell with insulated top and side walls and ran simulations with the stationary profiles of T, $\boldsymbol{v}$ and p from Figure S17 as initial conditions. For this series of simulations, we observed that the flow pattern

underwent multiple qualitative changes before eventually decaying, and that its direction (anticlockwise in the simulated region) was not preserved throughout its evolution. Thus, we can conclude that for teflon substrates with BDD annular bands under transient conditions, the flow pattern with upwelling at $r = 0$ is more stable than its approximate reflection with respect to $z = h_s$, despite the fact that the two are equivalent in stability under stationary conditions.

1B. Solution warmer than substrate at $t = 0$ ($\Delta T < 0$)

Homogeneous BDD substrate

The maximum flow velocity for this case is of the order of $\sim 10^{-9}$ m·s^{-1}, independent of the order of elements used for T (Figure S19A, Figure S20A), thereby making convective heat transfer negligible, as seen in the temperature profile within the solution, as well as the $\Delta T_{av}(t)$, Figure S19B-C, Figure S20B-C. In this system, the solution temperature is expected to be stably stratified and observed flows are likely caused by numerical noise. For that reason, we will not discuss their stability here.

A

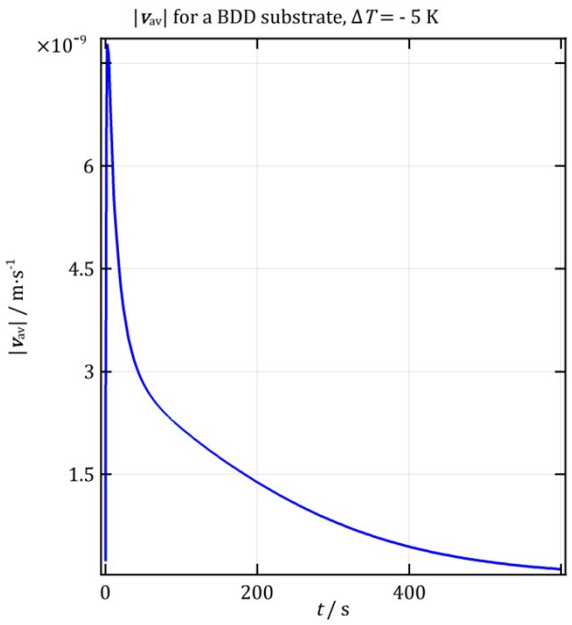

B

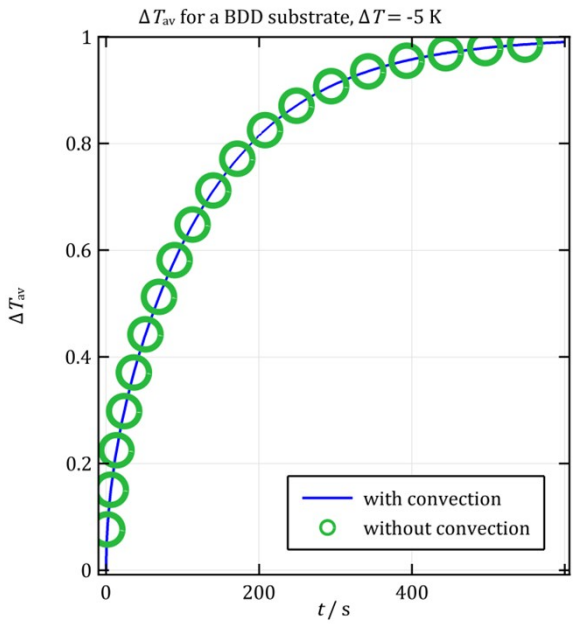

C

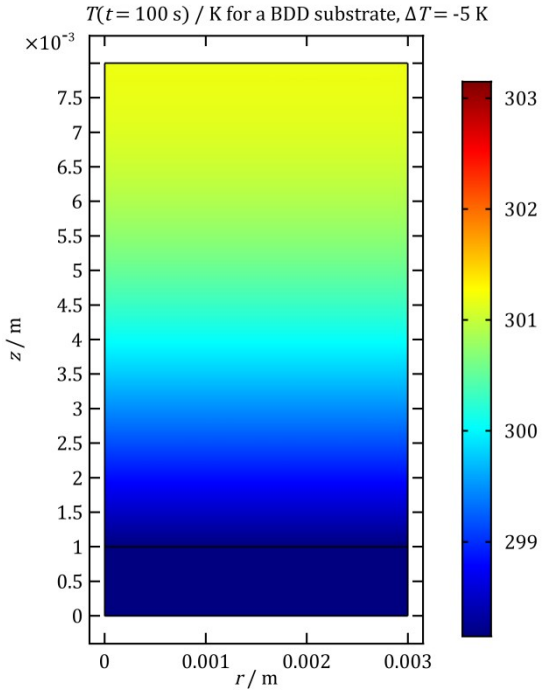

Figure S18. Results for a homogeneous BDD substrate obtained from a simulation that uses linear elements for T; the solution is initially warmer than the substrate and ΔT = - 5 K. **A** - volume-averaged velocity magnitude vs. time; **B -** volume-averaged dimensionless temperature difference; **C** - 'snapshot' of T at t = 100 s.

A

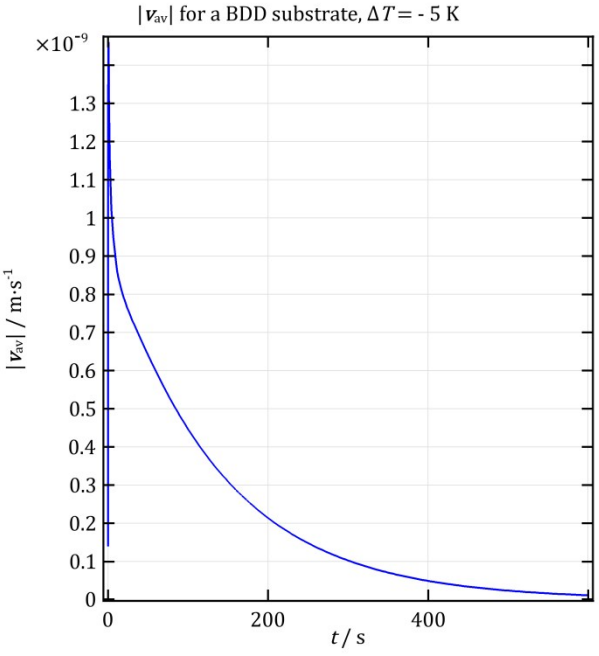

B

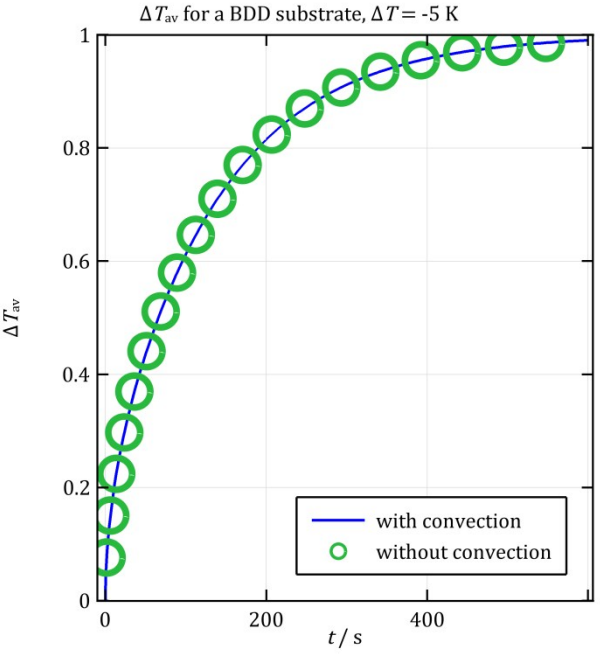

C

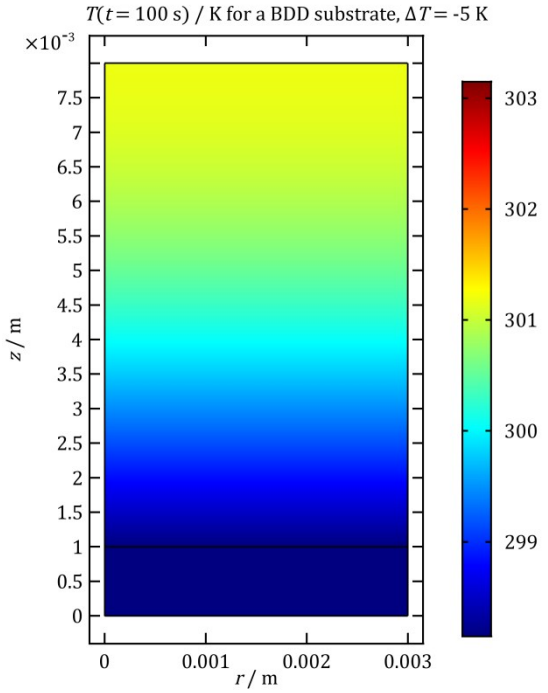

Figure S19. Results for a homogeneous BDD substrate obtained from a simulation that uses quadratic elements for T; the solution is initially warmer than the substrate and ΔT = - 5 K. **A** - volume-averaged velocity magnitude vs. time; **B -** volume-averaged dimensionless temperature difference; **C** - 'snapshot' of T at t = 100 s.

Homogeneous teflon substrate

In this case, the average solution velocity is again negligible – it reaches a peak value of just 10^{-10} to 10^{-9} m·s^{-1}, depending on whether linear or quadratic elements are used, see Figure S20A-Figure S21A. The convective flow is again likely due to numerical noise and is not sufficiently intense to affect the heat transfer, as demonstrated by the plots of ΔT_{av} versus t in Figure S20B-Figure S21B and the temperature profiles in Figure S20C-Figure S21C. As we are not interested in flows of such low velocity, we will not test their stability here.

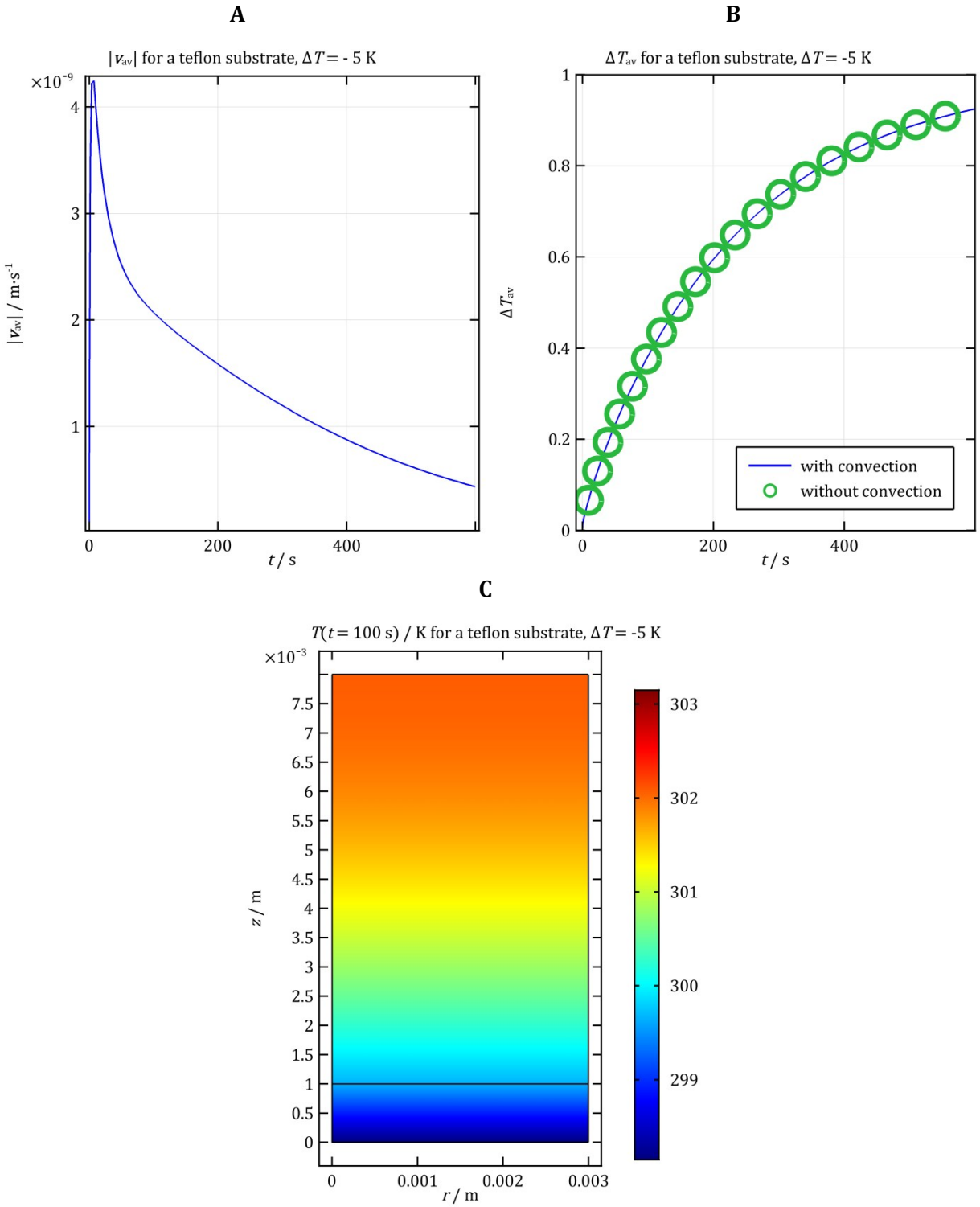

Figure S20. Results for a homogeneous teflon substrate obtained from a simulation that uses linear elements for T; the solution is initially warmer than the substrate and ΔT = - 5 K. **A** - volume-averaged velocity magnitude vs. time; **B -** volume-averaged dimensionless temperature difference; **C** - 'snapshot' of T at t = 100 s.

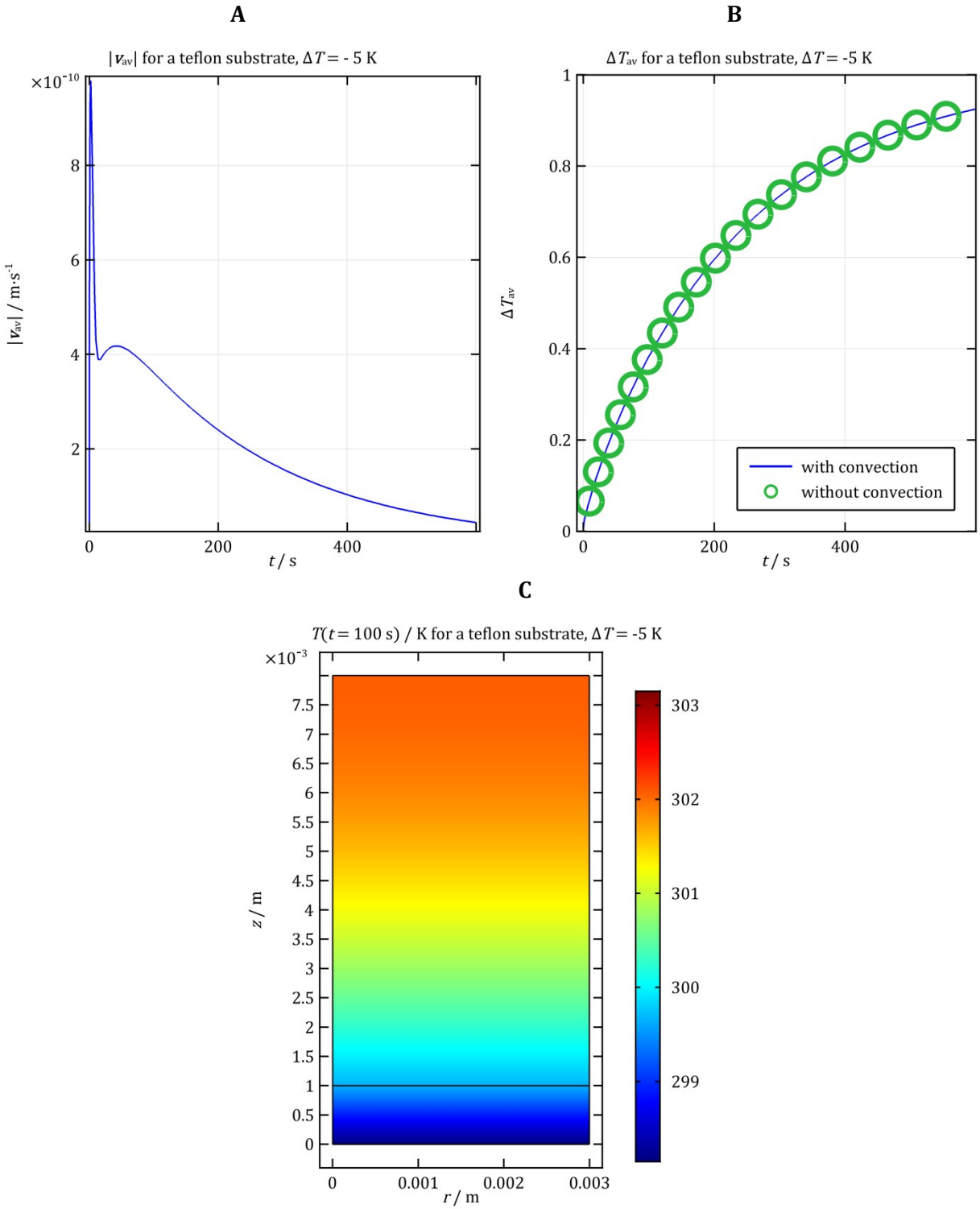

Figure S21. Results for a homogeneous teflon substrate obtained from a simulation that uses quadratic elements for T; the solution is initially warmer than the substrate and ΔT = - 5 K. **A** - volume-averaged velocity magnitude vs. time; **B -** volume-averaged dimensionless temperature difference; **C** - 'snapshot' of T at t = 100 s.

BDD substrates with teflon annular bands

In Figure S22, we present the average velocity, as well as 'snapshots' of $\boldsymbol{v}$ and T for BDD substrates with teflon annular bands situated within cells with insulated side and top walls at ΔT = -5 K. Notably, as Figure S22A illustrates, the intensity of the flow strongly depends on the width of the insulating annular band – the maximum velocity is $8.5\text{x}10^{-8}$ m·s^{-1} for d_{band}/r_{cell} = 1/27, $7.7\text{x}10^{-7}$ m·s^{-1} for d_{band}/r_{cell} = 1/9 and $5.1\text{x}10^{-6}$ m·s^{-1} for d_{band}/r_{cell} = 1/3. However, as seen in Figure S23, for all of the studied values of d_{band}, the convective flow within the solution has no appreciable effect on the overall heat transfer within the solution.

For the purpose of verifying our results, we also performed the same simulations with quadratic elements for T. This lead only to a quantitative difference in the observed toroidal rolls, namely an increase in $|\boldsymbol{v}_{av}|_{max}$ of 1.3%, 0.8% and 5.3% for d_{band}/r_{cell} = 1/3, 1/9 and 1/27, respectively. The variability of $|\boldsymbol{v}_{av}|_{max}$ with the element order is likely due to the different numerical accuracy of the two schemes. The comparatively large deviation for d_{band} = 1/27·r_{cell} is unimportant as for such a thin band, the flows within the solution are negligible and contain high levels of noise.

A

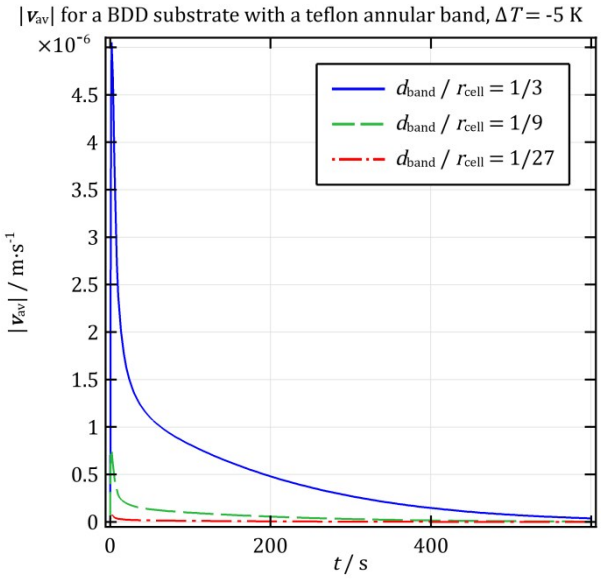

B

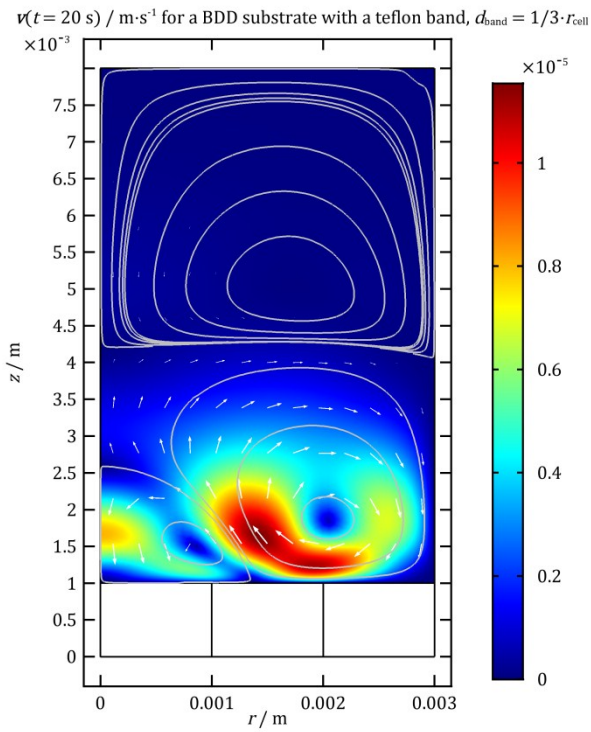
v(t = 20 s) / m·s-1 for a BDD substrate with a teflon band, dband = 1/3·rcell
×10-3
z / m
r / m
×10-5

C

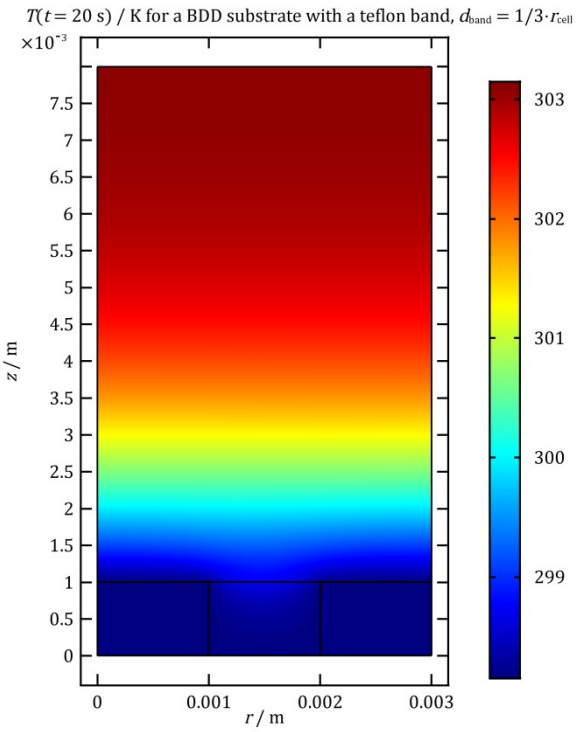
T(t = 20 s) / K for a BDD substrate with a teflon band, dband = 1/3·rcell
×10-3
z / m
r / m

D

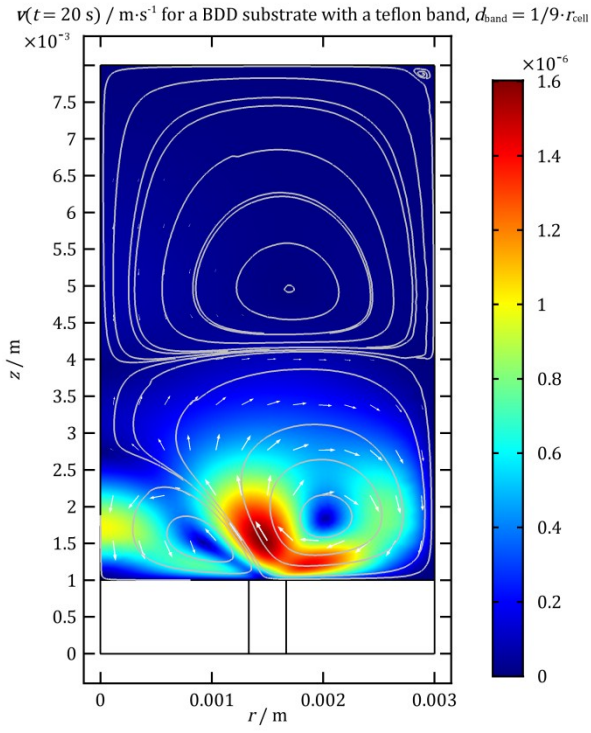
v(t = 20 s) / m·s-1 for a BDD substrate with a teflon band, dband = 1/9·rcell
×10-3
z / m
r / m
×10-6

E

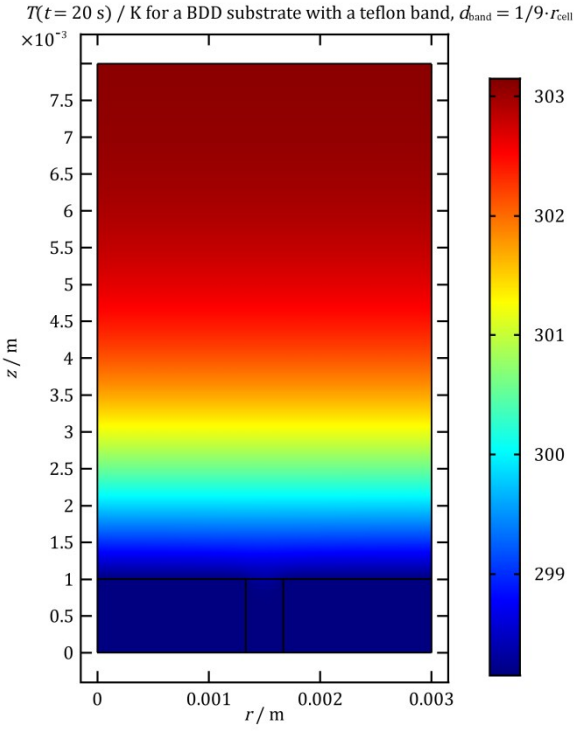
T(t = 20 s) / K for a BDD substrate with a teflon band, dband = 1/9·rcell
×10-3
z / m
r / m

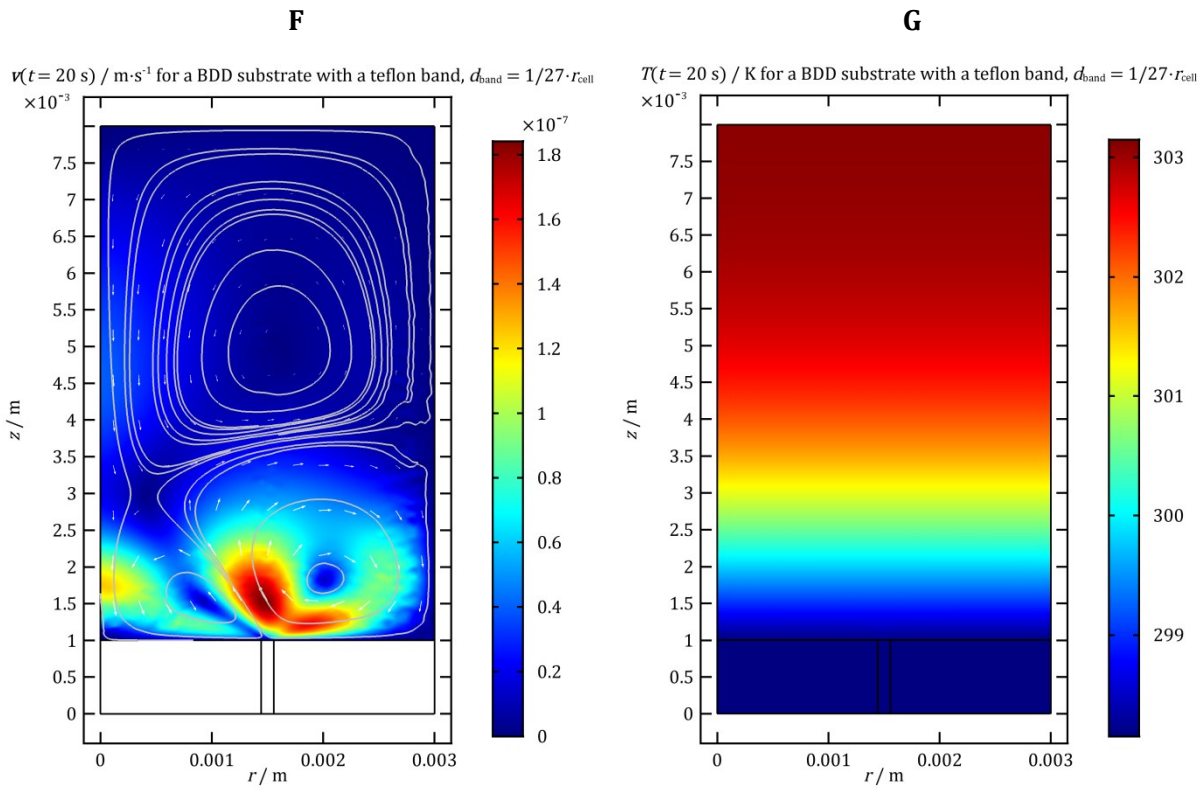

Figure S22. Results for a BDD substrate with a teflon band for simulations in which the solution is initially warmer than the substrate (ΔT = - 5 K). **A** – volume-averaged velocity magnitude. **B**, **D**, **F** – velocity distribution and streamlines illustrating the convective rolls for d_{band}/r_{cell} = 1/3, 1/9 and 1/27 taken at t = 20 s; **C**, **E** and **G** –$T(t$ = 20 s) for d_{band}/r_{cell} = 1/3, 1/9 and 1/27.

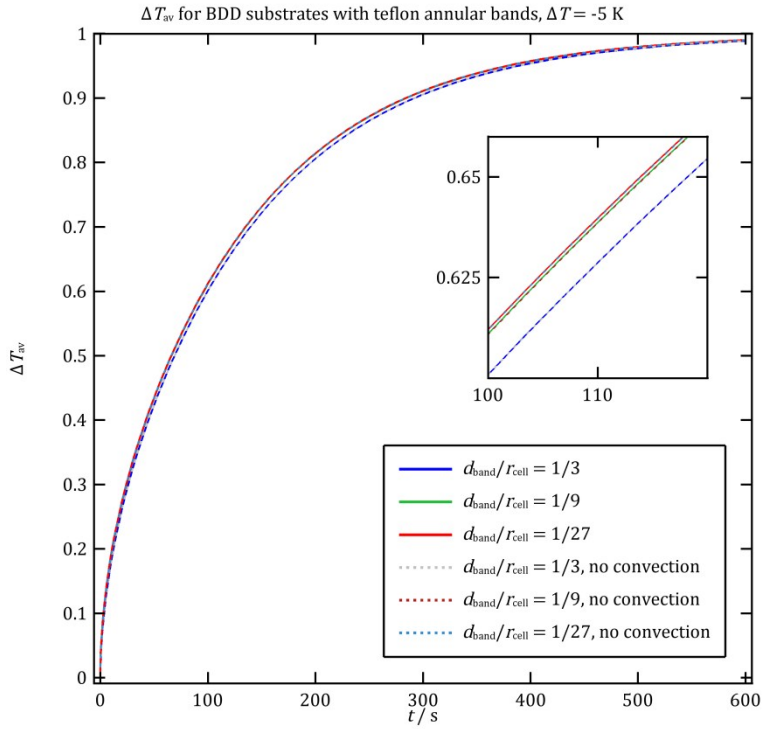

Figure S23. $\Delta T_{av}(t)$ for BDD substrates with teflon annular bands compared against simulations involving no convection, ΔT = - 5 K.

Stability tests

We ran simulations with the boundary condition (29) to study the stationary state for a conducting substrate with an insulating band. The simulations cover a time period of 300 s for the three band widths studied elsewhere in the text - see Figure S24 for a plot of the average velocity in the solution as a function of time. The velocity for bands of width $1/9 \cdot r_{cell}$ and $1/27 \cdot r_{cell}$ is of the order of 10^{-7} m·s^{-1} or below (see Figure S24A), as is the case for a cell with insulated walls. These flows contain high levels of numerical noise and are not of interest for our study.

In the stationary flow pattern for $d_{band} = 1/3 \cdot r_{cell}$, illustrated in Figure S24B, the flow is identical to that seen in a cell with an insulated top wall – in the simulated region (see Figure 1), there is a clockwise main roll occupying the space between r_1 and r_{cell} along the radial coordinate and between $h_s + h_{cell}/2$ and $h_s + h_{cell}$ along the normal. As with a cell with thermally insulated walls (Figure S22D), there are two additional rolls - one in the region $r \in [0, r_1]$ and one that occupies the upper half of the cylinder. For both of them, the flow is much less intense than in the main roll, and is in the opposite direction.

A

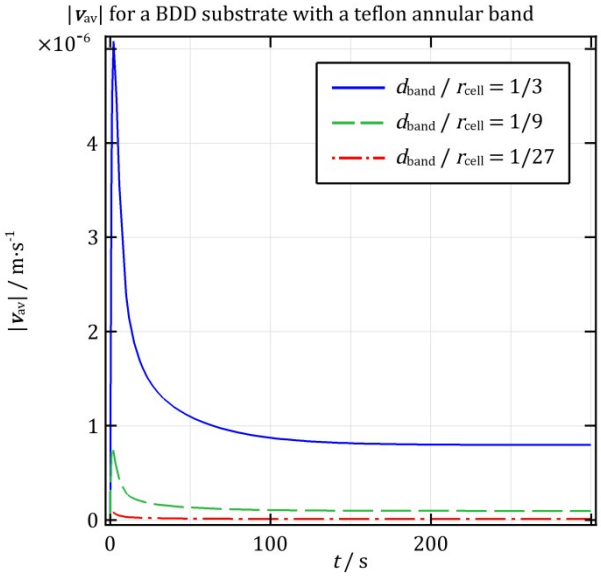

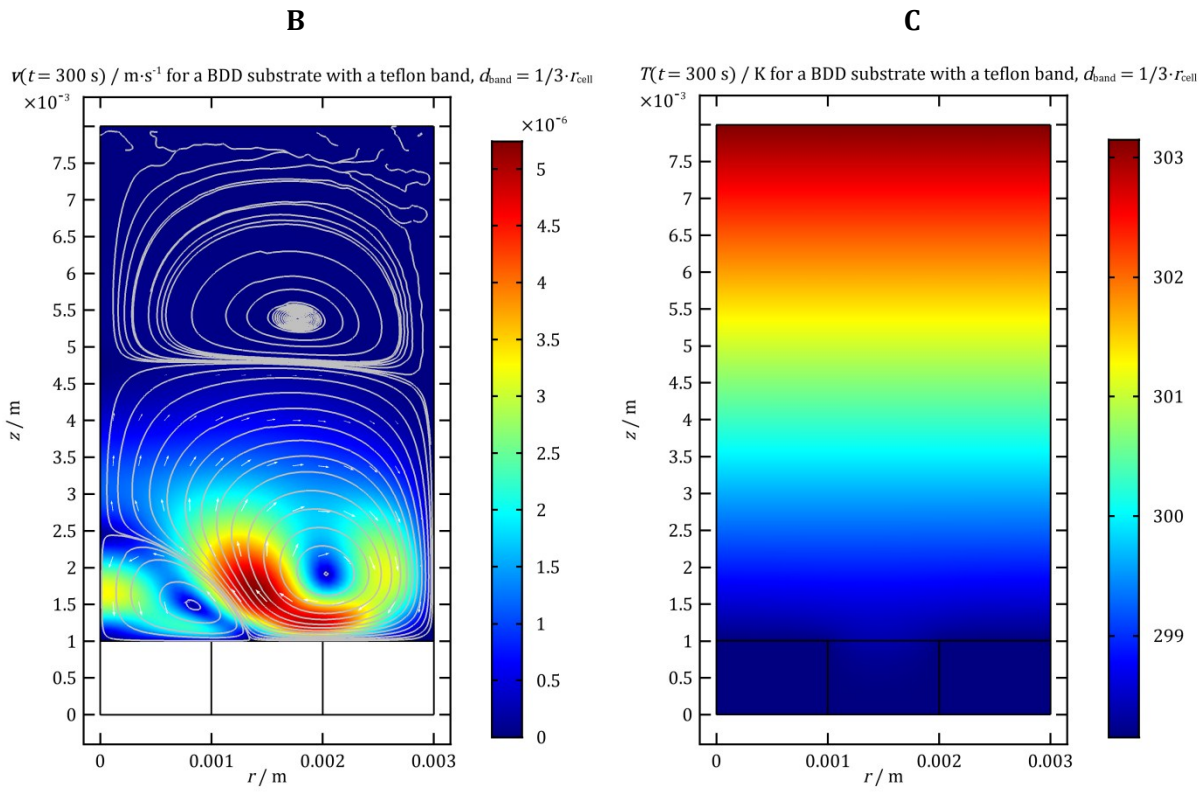

Figure S24. Results for simulations with a fixed temperature difference between the top and bottom cell walls, The substrate, which is initially colder than the solution (ΔT = - 5 K), is made of BDD and has a teflon annular band. **A** – volume-averaged velocity magnitude. **B** – $\boldsymbol{v}(t$ = 300 s) and streamlines and **C** –$T(t$ = 300 s) for d_{band}/r_{cell} = 1/3 at t = 300 s.

We tested whether a flow in which the direction of movement in the rolls is reversed is stable for this system. To this end, we used the stationary distributions (taken at t = 300 s) of $\boldsymbol{v}$, T^{L} and p from a simulation of the 'inverse' configuration with d_{band}/r_{cell} = 1/3 as initial conditions (see Figure S28 below). For the temperature of the solid, we used the stationary distribution as calculated at t = 300 s for a substrate with an insulating band (seen in Figure S24 for d_{band}/r_{cell} = 1/3). In contrast to the case with $\Delta T > 0$, here the direction of the flow is reversed on a timescale of ~10 s and the pattern obtained from simulations with an initially stagnant solution is restored. This is illustrated in Figure S25, where the drop in the average velocity corresponds to the period when the intensity of fluid motion in the rolls drops before they reverse direction. Thus, we can conclude that for a teflon substrate with a BDD annular band at $\Delta T < 0$, the stability of the rolls is influenced by the direction of flow within them. The pattern in which the flow direction in all rolls is reversed with respect to the ones pictured in Figure S24, is unstable for this substrate, but, as we have shown below, is stable for substrates possessing the 'inverse' structure.

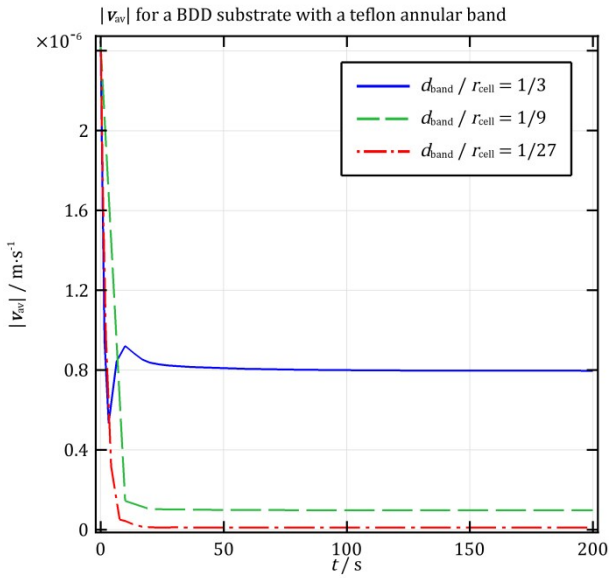

Figure S25. Volume-averaged velocity magnitude $|\boldsymbol{v}_{av}(t)|$ for BDD substrates with teflon annular bands from simulations with a fixed temperature difference of ΔT = –5 K between the bottom and top cell walls. The initial conditions for $\mathbf{v}$, T^{L} and p correspond to direction of the fluid motion in the rolls opposite to that obtained from simulations of the same substrate with an initial condition for a stagnant solution and d_{band}/r_{cell} = 1/3(see Figure S24). T^{S} is taken from the stationary prediction of the simulation of a BDD substrate with a teflon annular band with the respective value of d_{band} that employs stagnant initial conditions. Note the drastic change in the average solution velocity – this corresponds to a reversal of the direction of flow and establishment of a pattern resembling the ones in Figure S23-Figure S24.

Teflon substrates with BDD annular bands

Figure S26 presents results for teflon substrates with BDD annular bands at ΔT = -5 K, complementing Figure 6 from the main text by giving 'snapshots' of $\boldsymbol{v}$ and T for d_{band} = 1/9 and 1/27 near the moment the average velocity reaches its peak value. In Figure S27, by comparing with ΔT_{av} for purely conductive heat transfer, we show that, despite the considerable velocities within the solution ($\boldsymbol{v}_{av} \sim 10^{-6}$ m·s^{-1}), none of the flows have a significant influence on the solution temperature.

To verify our results, we ran the same simulations with quadratic elements for T and observed no difference in the flow pattern. We did, however, observe small variations in $|\boldsymbol{v}_{av}|_{max}$ as in our other simulations of substrates with annular bands – increasing the shape function order leads to an increase in peak height of 1.4 % for d_{band}/r_{cell} = 1/3, and a decrease of 2.7% and 1.1% for d_{band}/r_{cell} = 1/9 and 1/27, respectively.

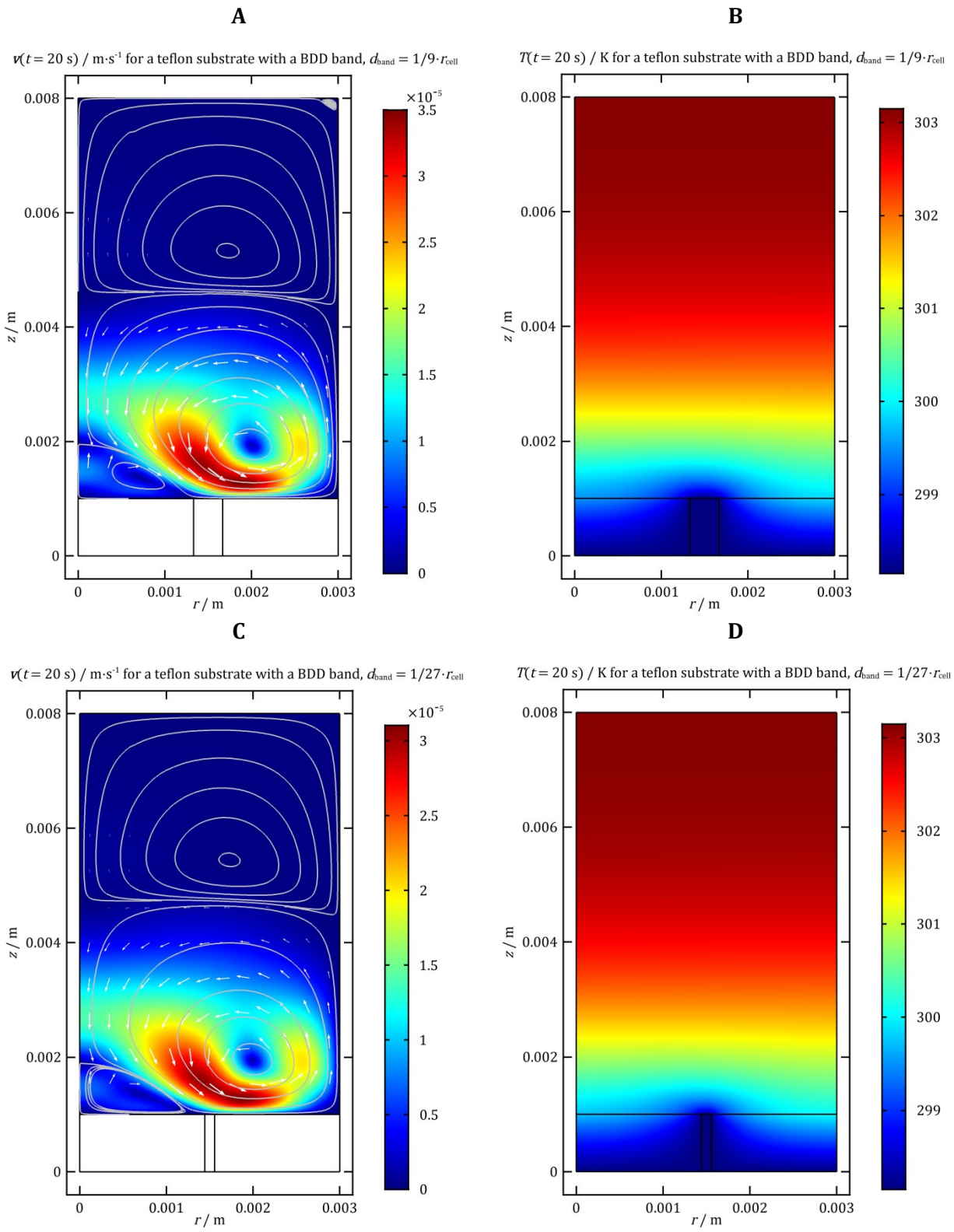

Figure S26. Results for a teflon substrate with a BDD band, The solution is initially warmer than the substrate (ΔT = -5 K). **A** and **C** – velocity distributions and streamlines at t = 20 s for d_{band}/r_{cell} = 1/9 and d_{band}/r_{cell} = 1/27; **B** and **D** – $T(t$ = 20 s) for d_{band}/r_{cell} = 1/9 and d_{band}/r_{cell} = 1/27.

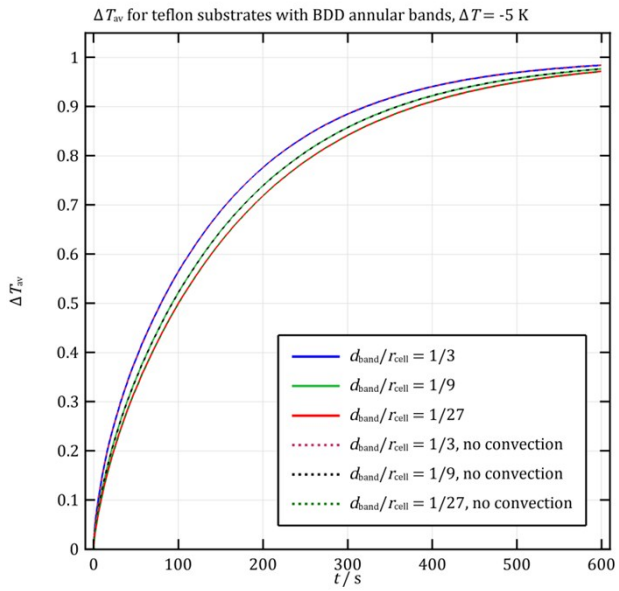

Figure S27. $\Delta T_{av}(t)$ for teflon substrates with BDD annular bands compared against simulations involving no convection, ΔT = - 5 K.

Stability tests

As we did for other configurations, we also studied the flow stability qualitatively by performing simulations with the fixed-temperature boundary condition (29) at the top wall rather than a condition for no normal heat flux. As illustrated in Figure S28, in all cases, we observed flows with a stationary average velocity of the order of 10^{-6} m·s^{-1} and a velocity distribution with a main anticlockwise roll and secondary clockwise ones identical to those from the simulations of cells with thermally insulated top walls.

A

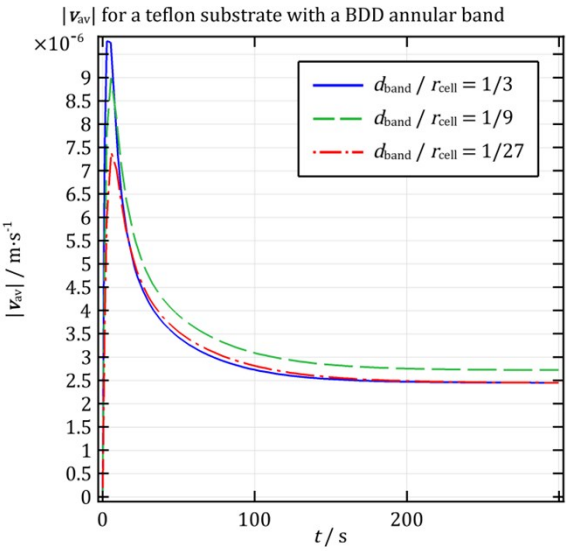

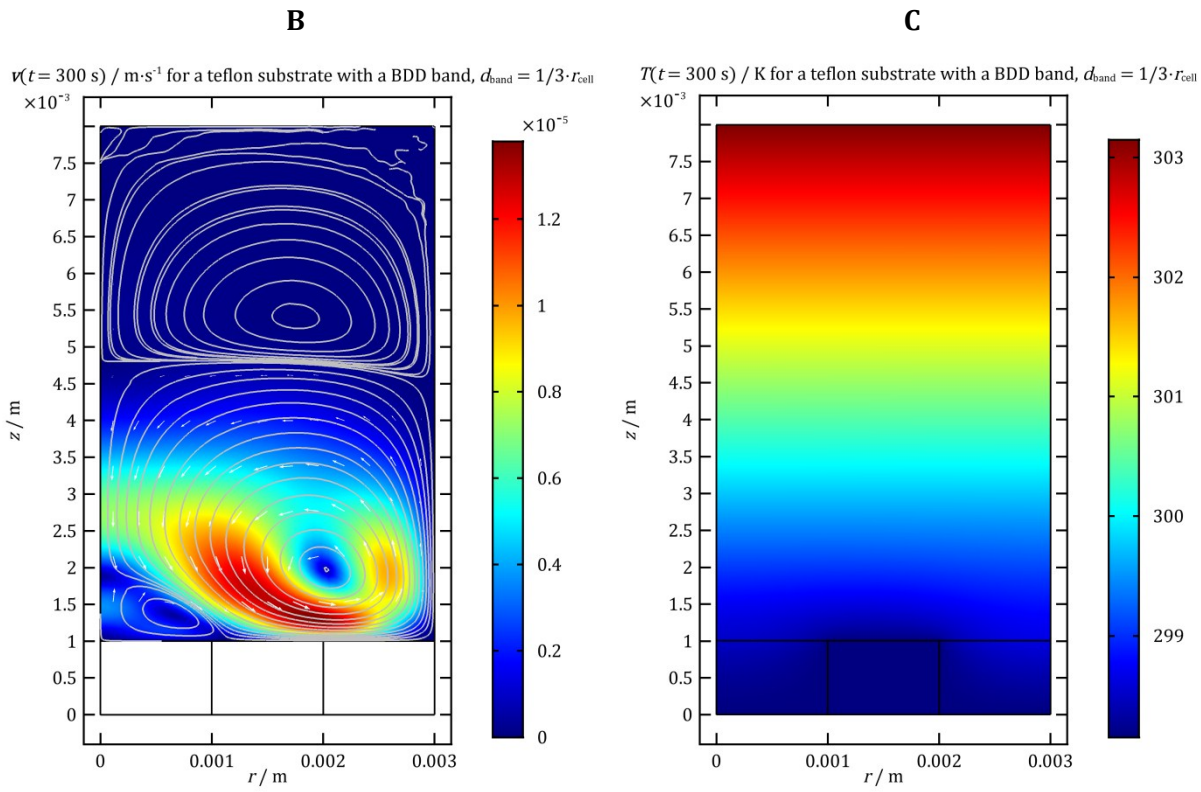

Figure S28. Results for simulations with a fixed temperature difference between the top and bottom cell walls, The substrate, which is made of teflon and has a BDD annular band, is initially colder than the solution (ΔT = - 5 K). **A** – volume-averaged velocity magnitude. **B** and **C** – velocity and temperature distributions for d_{band}/r_{cell} = 1/3 at t = 300 s.

We tested the stability of a flow pattern in which the direction of movement within the rolls is reversed. To that end, we ran simulations with the stationary distributions of $\boldsymbol{v}$, T^L and p for the 'inverse' configuration at d_{band}/r_{cell} = 1/3 as initial conditions. For T^S, we employed the stationary profile for a teflon substrate with a BDD annular band with the same d_{band} as the studied substrate. In these simulations, the flow reverses direction with respect to the initial conditions over a time scale of 10 s and reaches a stationary state analogous to that pictured in Figure S28 over a period of ~100 s (see Figure S29 for a plot of $|\boldsymbol{v}_{av}|$). From these results, we can conclude that the direction of flow within the convective rolls is an intrinsic feature of the convective patterns that develop in cells containing substrates teflon substrates with BDD annular bands, as is the case for the 'mirror' configuration.

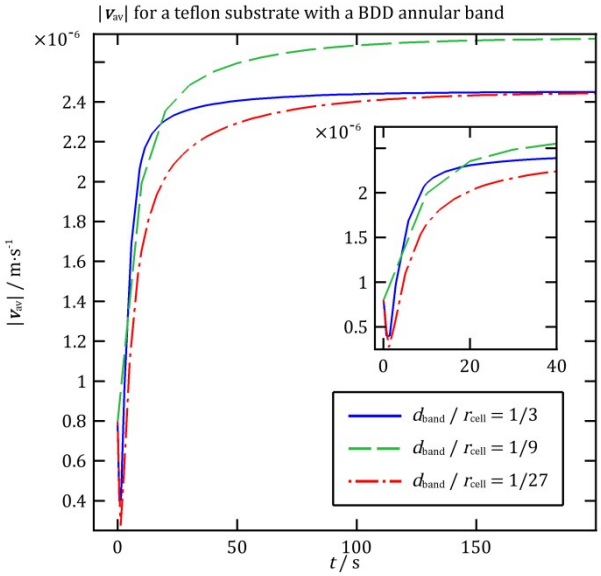

Figure S29. Volume-averaged velocity magnitude $|\boldsymbol{v}_{\mathrm{av}}(t)|$ for teflon substrates with BDD annular bands from simulations with a fixed temperature difference of ΔT = –5 K between the bottom and top cell walls. The initial conditions for $\mathbf{v}$, T^{L} and p correspond to direction of the fluid motion in the rolls opposite to that obtained from simulations of the same substrate with an initial condition for a stagnant solution. T^{S} is taken from the stationary prediction of the simulation of a teflon substrate with a BDD annular band with the respective width that employs stagnant initial conditions. Note the initial drop in the average solution velocity (inset) – this corresponds to a reversal of the direction of flow and a transition to a pattern resembling the ones in Figure S26 and Figure S28.

2. Simulations for r_{cell} = 8 mm

Due to the similarity with the discussion for the smaller cell, here we will not provide all details regarding the simulations of the larger cell. In particular, we will only discuss the stability analysis of the flows for r_{cell} = 8 mm where it differs substantially from the previous case.

In all simulations of the cell with r_{cell} = 8 mm, we set the pressure difference $\Delta p = p - p_0 + \rho z|g|$ at the point (r_{cell}, $h_{\mathrm{s}} + h_{\mathrm{cell}}$) to zero. This eliminates a contribution to the pressure that depends only on time and thus simplifies the numerical solution of the problem. As only the pressure gradient and not its absolute value matter for an incompressible fluid, this does not affect the physically meaningful quantities that are being solved for.

2A. Solution colder than substrate at t = 0 (ΔT > 0)

BDD substrate

Figure S30 illustrates the results for this system discussed in the main text with plots of $|\boldsymbol{v}_{\mathrm{av}}|$, ΔT_{av}. ‘Snapshots’ of the velocity and temperature at the vicinity of the three maxima in the volume-averaged velocity illustrate the main stages in the evolution of the flow.

A

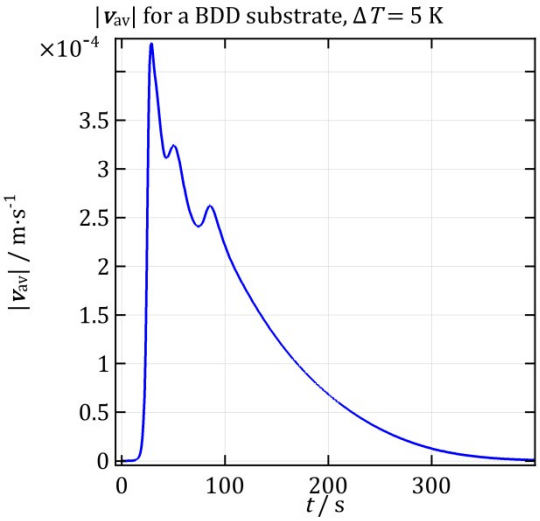
|v_{av}| for a BDD substrate, $\Delta T = 5$ K
×10⁻⁴
3.5
3
2.5
2
1.5
1
0.5
0
|v_{av}| / m·s⁻¹
0
100
200
300
t / s

B

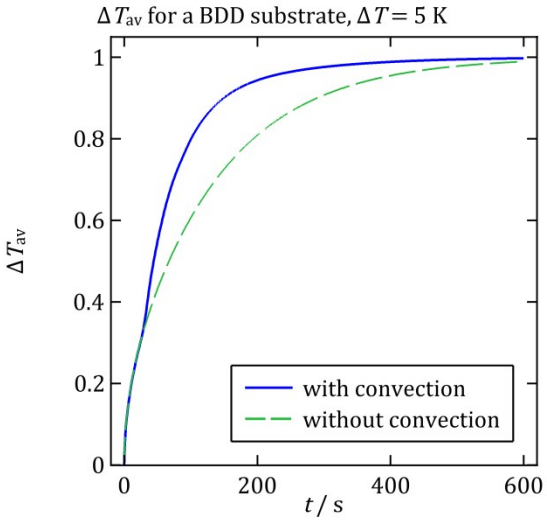
ΔT_{av} for a BDD substrate, $\Delta T = 5$ K
1
0.8
0.6
0.4
0.2
0
ΔT_{av}
with convection
without convection
0
200
400
600
t / s

C

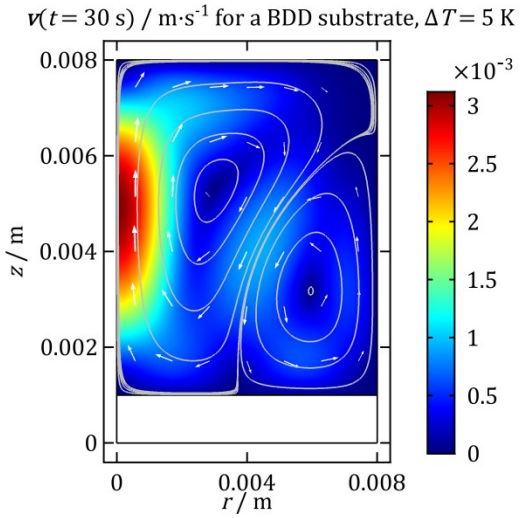
$v(t = 30$ s) / m·s⁻¹ for a BDD substrate, $\Delta T = 5$ K
0.008
0.006
0.004
0.002
0
z / m
×10⁻³
3
2.5
2
1.5
1
0.5
0
0
0.004
0.008
r / m

D

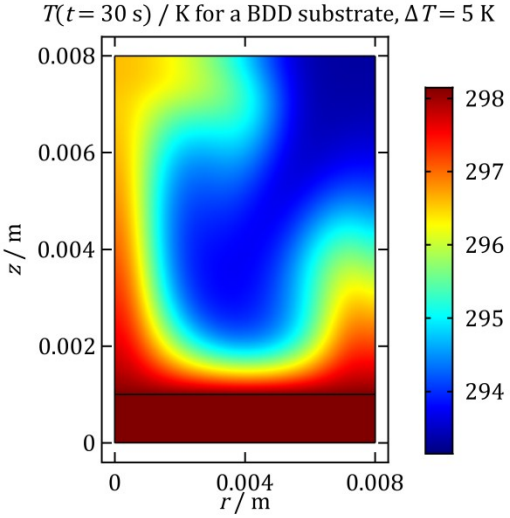
$T(t = 30$ s) / K for a BDD substrate, $\Delta T = 5$ K
0.008
0.006
0.004
0.002
0
z / m
298
297
296
295
294
0
0.004
0.008
r / m

E

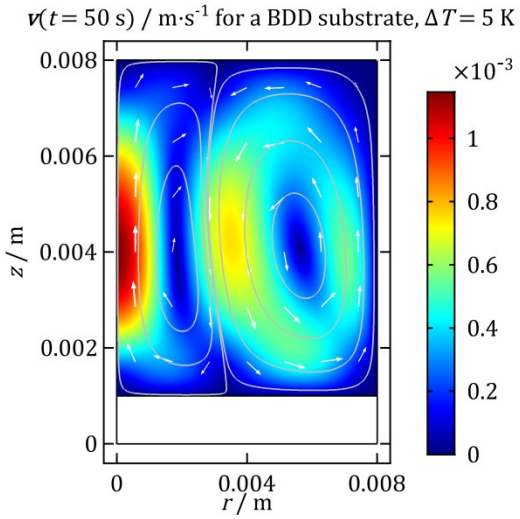
$v(t = 50$ s) / m·s⁻¹ for a BDD substrate, $\Delta T = 5$ K
0.008
0.006
0.004
0.002
0
z / m
×10⁻³
1
0.8
0.6
0.4
0.2
0
0
0.004
0.008
r / m

F

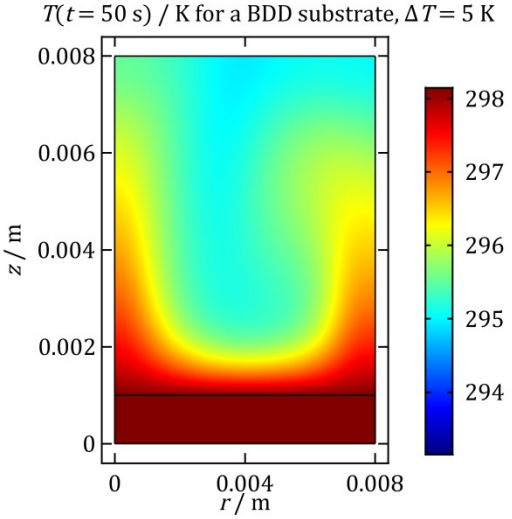
$T(t = 50$ s) / K for a BDD substrate, $\Delta T = 5$ K
0.008
0.006
0.004
0.002
0
z / m
298
297
296
295
294
0
0.004
0.008
r / m

G

H

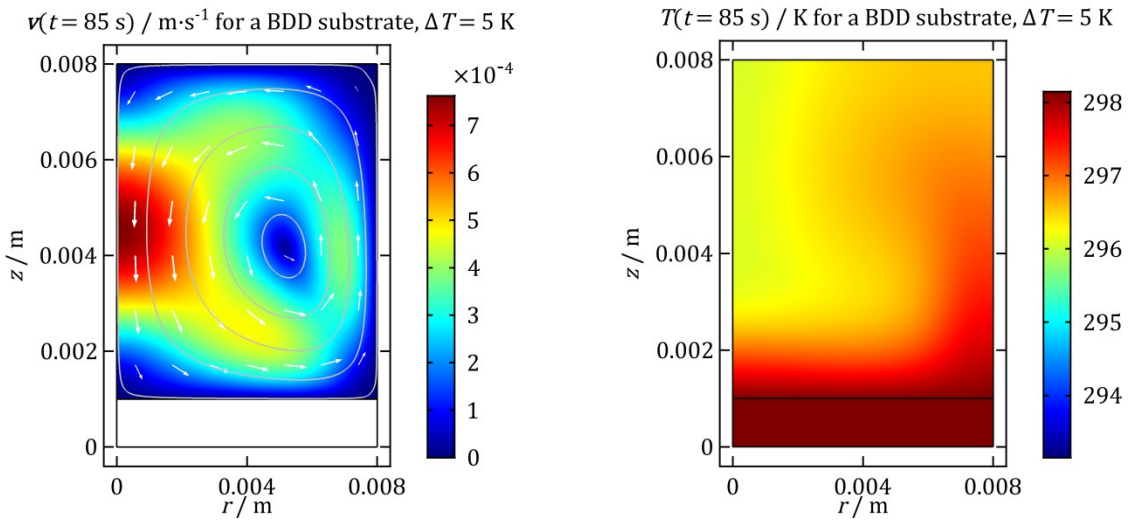

Figure S30. Results for a BDD substrate situated at the bottom of a cell of radius 8 mm (linear elements for T). The solution is initially colder than the substrate (ΔT = 5 K). **A** – $|\boldsymbol{v}_{av}|$ vs. t; **B** - volume averaged dimensionless ΔT_{av} vs. t; **C, E, G** – velocity distribution and streamlines illustrating the convective rolls taken at t = 30, 45 and 85 s; **D, F, H** –T at t = 30, 45 and 85 s.

Teflon substrate

Figure S31 and Figure S32 complement the discussion of our simulations of teflon substrates situated in cells with a radius of 8 mm. They represent the results obtained with linear and quadratic elements for T, respectively – note the difference in direction in the motion of the fluid, as well as the contrasting temperature distributions. For each case, the 'snapshots' of $\boldsymbol{v}$ and T are taken approximately at the moment of time corresponding to the main peak in the average solution velocity.

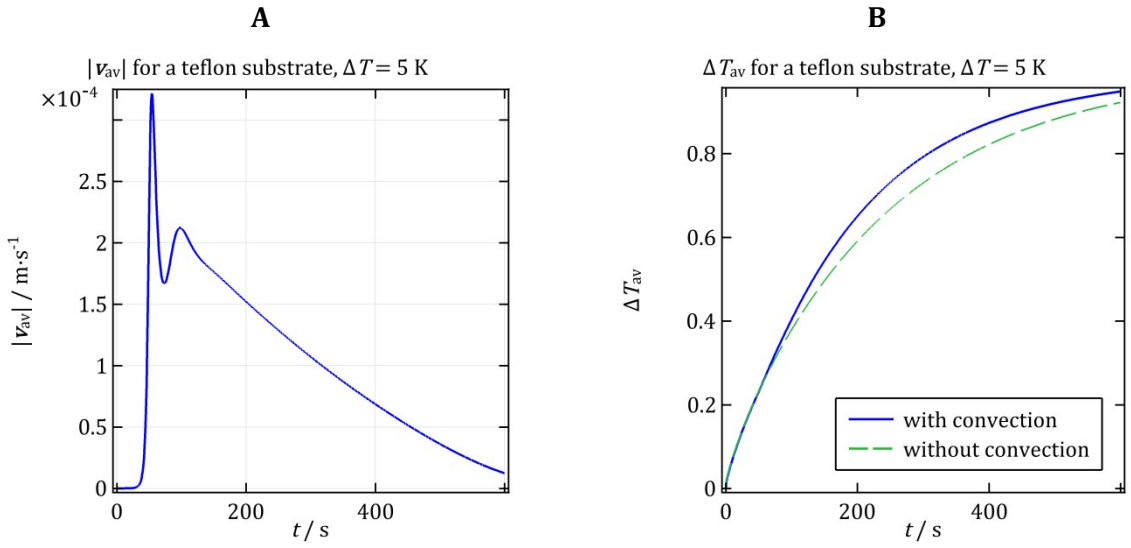

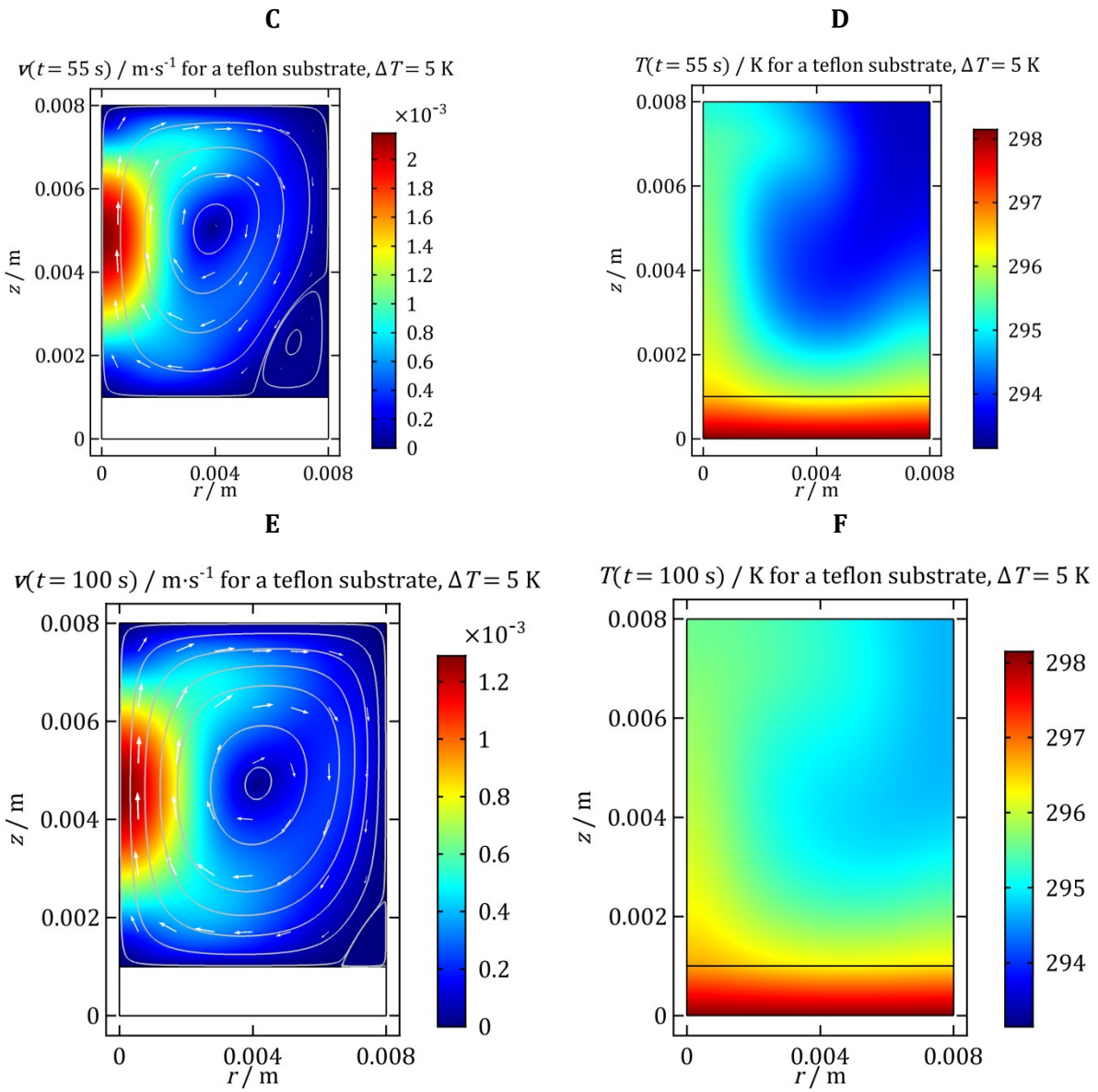

Figure S31. Results for a teflon substrate situated at the bottom of a cell of radius 8 mm obtained using linear shape functions for T. The solution is initially colder than the substrate (ΔT = 5 K). **A** – $|v_{av}|$ vs. t; **B** - volume averaged dimensionless ΔT_{av} vs. t; **C** and **E** – velocity distribution and streamlines illustrating the main and secondary convective rolls at t = 55 and 100 s; **D** and F – temperature distribution at t = 55 and 100 s.

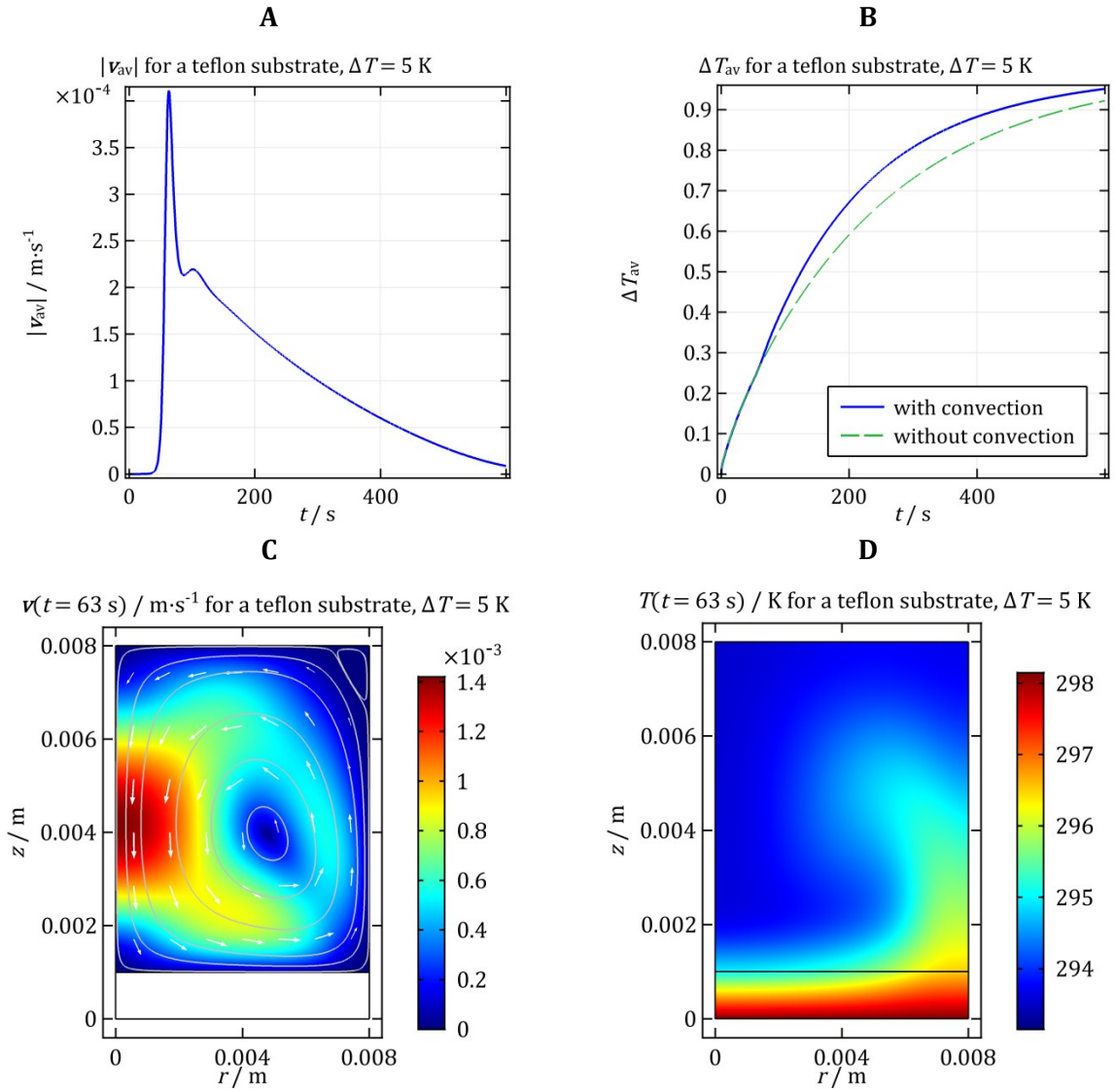

Figure S32. Results for a teflon substrate situated at the bottom of a cell of radius 8 mm obtained using quadratic shape functions for T. The solution is initially colder than the substrate (ΔT = 5 K). **A** – $|\boldsymbol{v}_{av}|$ vs. t; **B** - volume averaged dimensionless ΔT_{av} vs. t; **C** – velocity distribution and streamlines illustrating the main and secondary convective rolls at t = 63 s; **D** – temperature distribution at t = 63 s.

BDD substrate with a teflon annular band

We studied the stability of the flows arising in this system using a methodology very similar to the one we described for substrates with the same structure situated at the bottom of cells with r_{cell} = 3 mm. The only point of difference was that to test the stability of the flow pattern with upwelling at r = 0, we used the velocity, temperature and pressure distributions obtained for long times from our simulation of a teflon substrate with a BDD annular band utilising the fixed-temperature boundary condition (29). As before, the initial condition for the temperature distribution within the solid substrate was taken from the steady-state limit of the simulation of a BDD substrate with a teflon annular band with a stagnant initial solution.

As we pointed out in the main text, our tests indicate that for this system, the roll with direction of flow opposite to that illustrated in Figure 8C is unstable, as is the case for r_{cell} = 3 mm.

Teflon substrate with a BDD annular band

Figure S33 presents plots of $|\boldsymbol{v}_{av}|$, ΔT_{av} and 'snapshots' of the velocity and temperature for teflon substrates with BDD annular bands discussed in the main text.

A

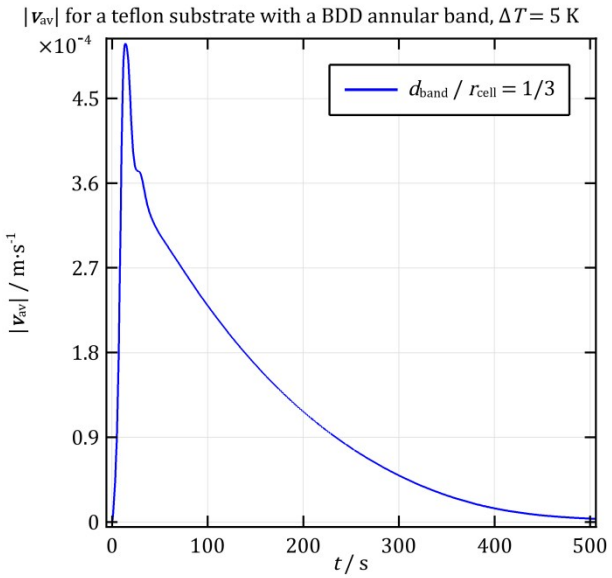

B

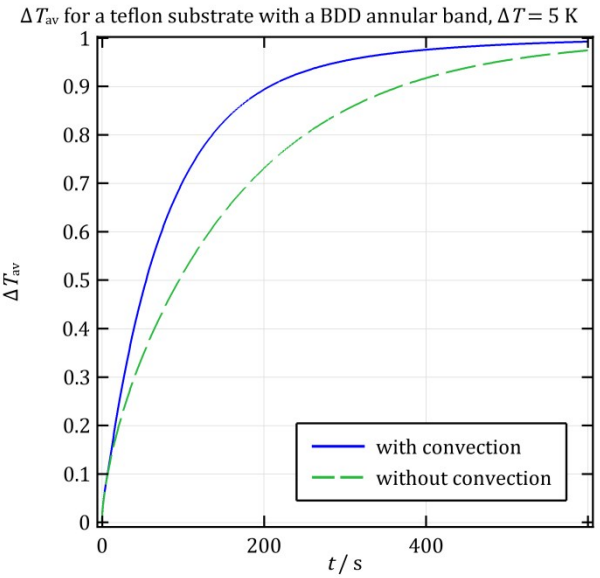

C

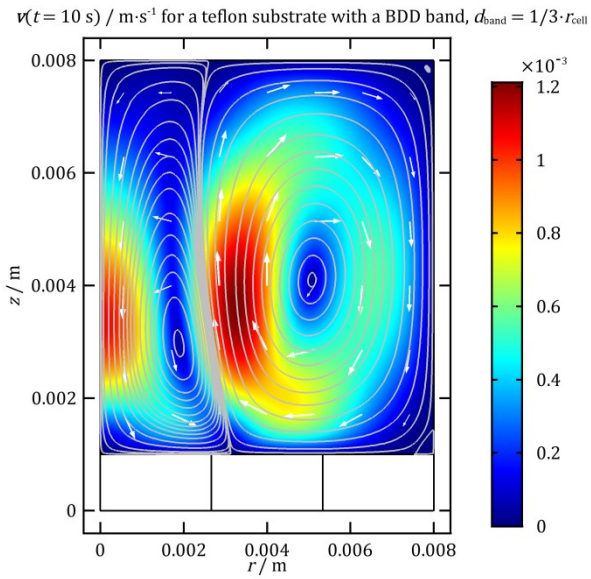

D

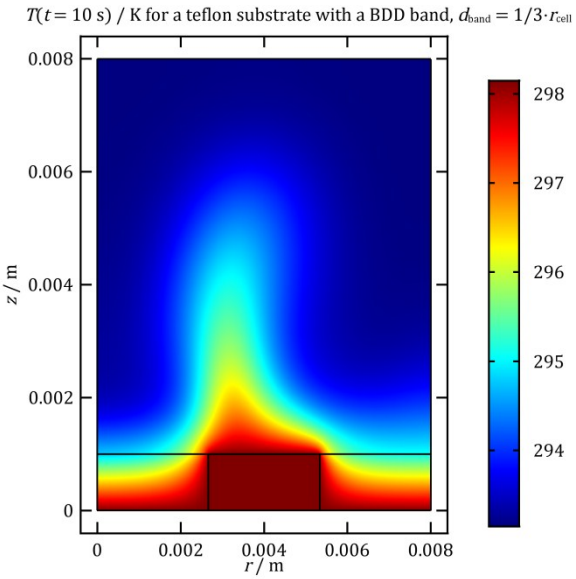

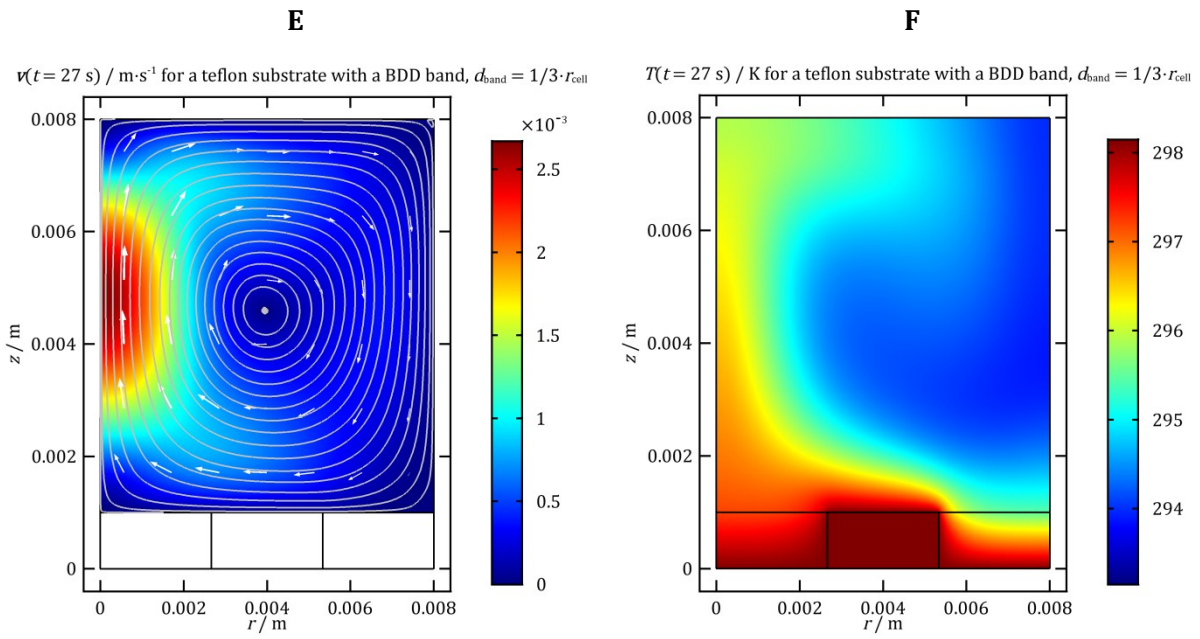

Figure S33. Results for a teflon substrate with a BDD annular band (d_{band}/r_{cell} = 1/3) situated at the bottom of a cell of radius 8 mm. The solution is initially colder than the substrate (ΔT = 5 K). **A** – $|\boldsymbol{v}_{av}|$ vs. t; **B** - volume averaged dimensionless ΔT_{av} vs. t; **C** – velocity distribution and streamlines illustrating the two convective rolls that arise in the system at t = 10 s, corresponding to the maximum in velocity; **D** – temperature distribution at t = 10 s, exhibiting a sharp maximum at $r \sim r_1$. **E**, **F** – illustrations of the convective flow that arises at long times and the temperature distribution corresponding to it.

We tested the stability of the flow in this system in the same way as we did for r_{cell} = 3 mm. As in the case of BDD substrates with teflon annular bands at r_{cell} = 8 mm, the only difference was that to establish whether the roll with direction opposite to that in Figure S33 is stable, we used the steady-state distributions of $\boldsymbol{v}$, T^L and p obtained from the simulation of the 'inverse' configuration with eq. (29) as the top boundary condition. For T^S, we used the distribution from the steady-state limit of the simulation of a teflon substrate with a BDD annular band and a stagnant initial solution.

As we have noted in the main text, these tests indicate that the roll with direction opposite to that shown in Figure S33 is unstable, as is the case for r_{cell} = 3 mm.

2B. Solution warmer than substrate at t = 0 (ΔT < 0)

BDD substrate with a teflon annular band

Figure S34 illustrates the results for this system discussed in the main text with plots of $|\boldsymbol{v}_{av}|$, ΔT_{av} and 'snapshots' of the velocity and temperature. Comparison with Figure S24 shows that the increase of r_{cell} leads to an increase in $|\boldsymbol{v}_{av}|$, but no qualitative difference in the system's behaviour.

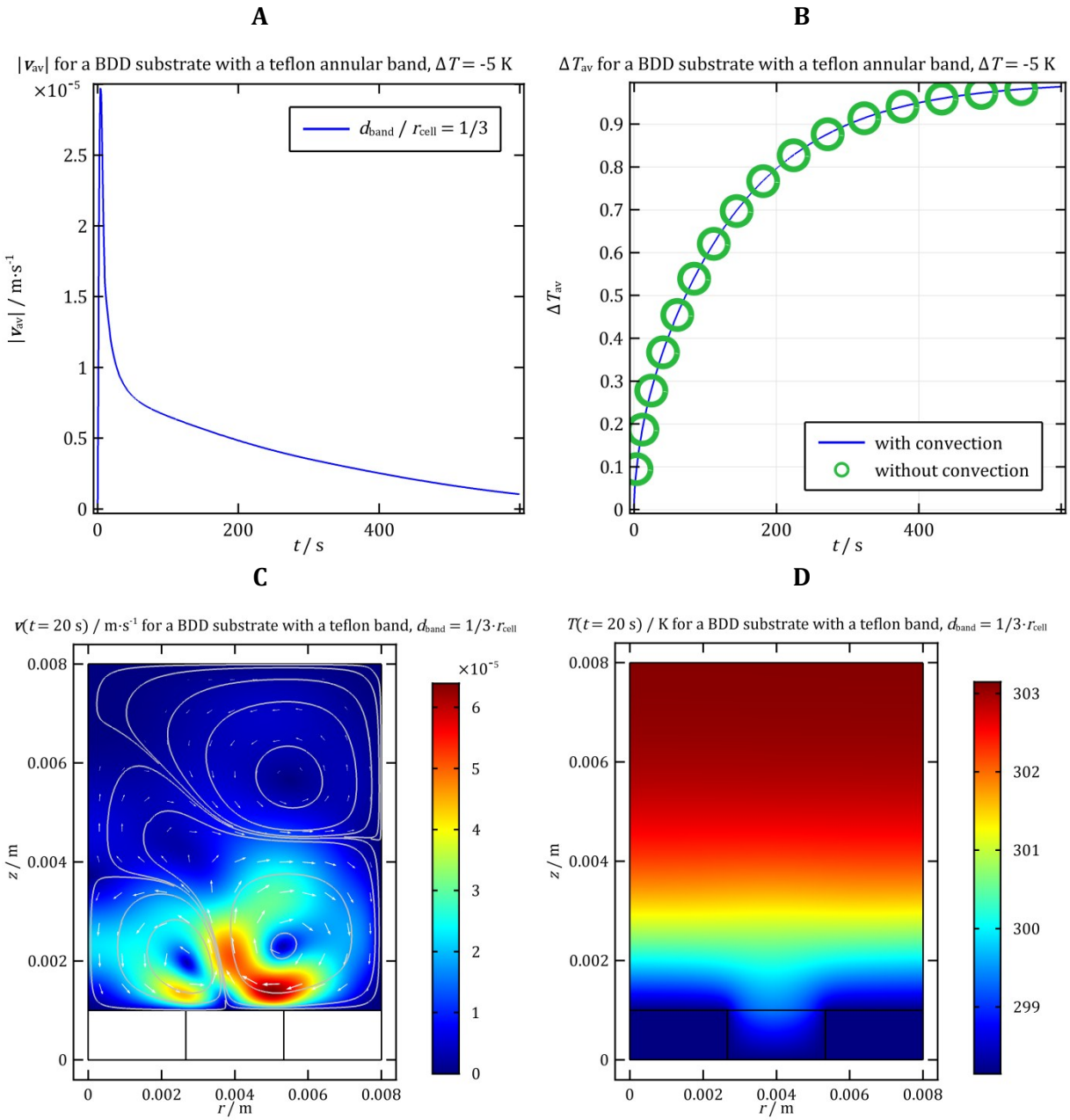

Figure S34. Results for a BDD substrate with a teflon band (d_{band}/r_{cell} = 1/3) situated at the bottom of a cell of radius 8 mm. The solution is initially warmer than the substrate (ΔT = - 5 K). **A** – $|\boldsymbol{v}_{av}|$ vs. t; **B** - volume averaged dimensionless ΔT_{av} vs. t; **C** – velocity distribution and streamlines illustrating the convective rolls taken at t = 20 s; **D** –$T(t$ = 20 s).

Teflon substrate with a BDD annular band

Figure S35 illustrates the results for this system discussed in the main text with plots of $|\boldsymbol{v}_{av}|$, ΔT_{av} and 'snapshots' of the velocity and temperature. As with the 'inverse' substrate structure, the analogy with the case of the smaller cell is complete, the only difference being the lower velocity magnitude for the latter – see Figure 6 for comparison.

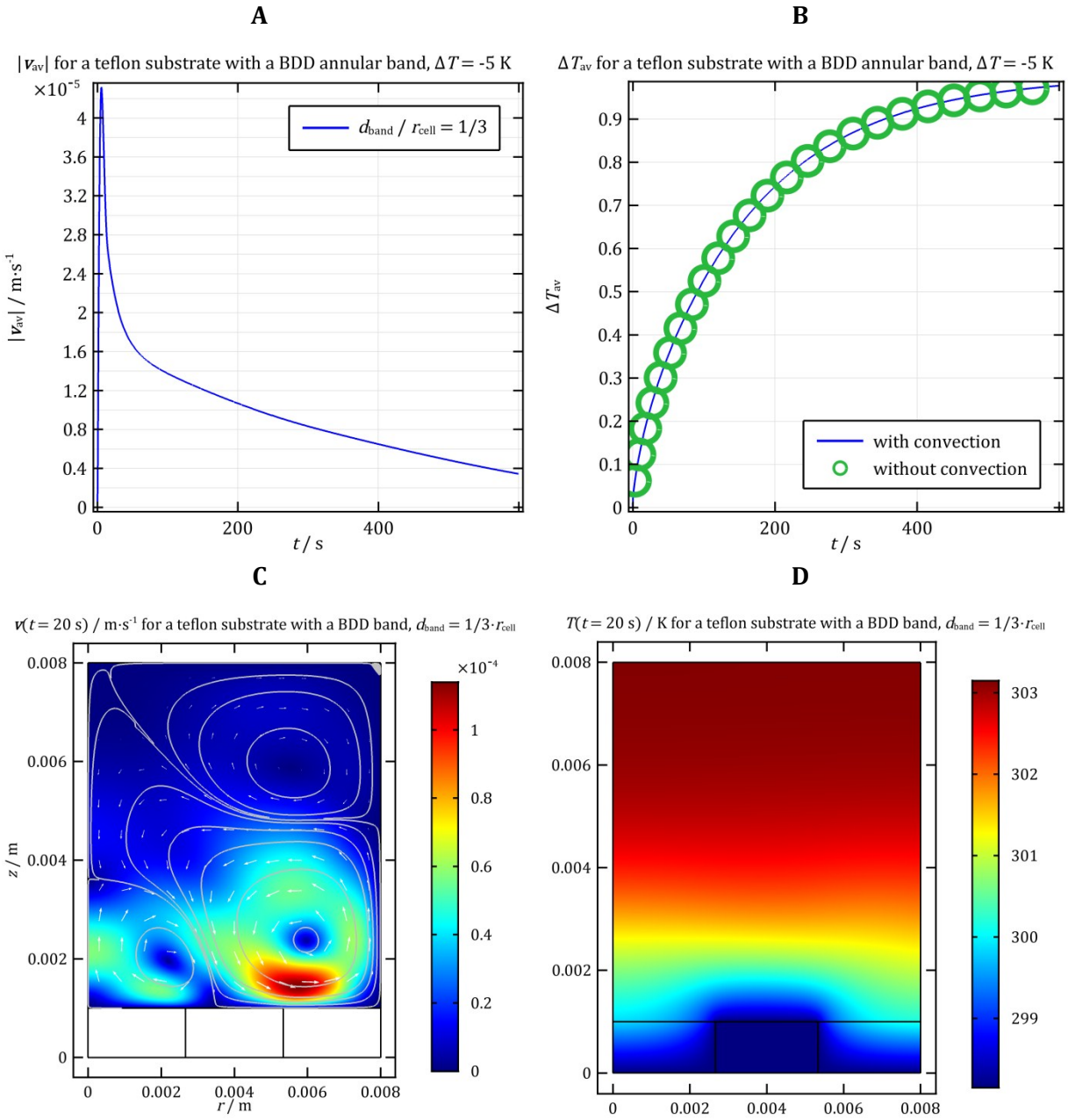

Figure S35. Results for a teflon substrate with a BDD band (d_{band}/r_{cell} = 1/3) situated at the bottom of a cell of radius 8 mm. The solution is initially warmer than the substrate (ΔT = - 5 K). **A** – $|\boldsymbol{v}_{av}|$ vs. t; **B** - volume averaged dimensionless ΔT_{av} vs. t; **C** – velocity distribution and streamlines illustrating the convective rolls taken at t = 20 s; **D** –$T(t$ = 20 s).

II. Meshing

The numerical solution of the governing equations via the finite element method requires the meshing of the simulated region of space. Like the rest of the numerical procedure, this was implemented in COMSOL Multiphysics. For the liquid next to the boundaries with a no-slip condition, we employ COMSOL's 'boundary layer' mesh, which consists of a grid of quadrilaterals that expands in the direction normal to the interface; for the bulk liquid phase and the solid, we use a free triangular mesh. These settings

result in 11022 and 22058 elements in total for homogeneous substrates for r_{cell} = 3 and 8 mm, respectively. In the case of annular bands, we set the number of elements at the band-solution interface ($z = h_s$, $r \in [r_1, r_1 + d_{band}]$) to 75 in order to guarantee that the velocity and temperature distributions in the vicinity of the band are adequately described. The total number of elements in the mesh is 17169 for d_{band}/r_{cell} = 1/3, 19947 for d_{band}/r_{cell} = 1/9, and 22325 for d_{band}/r_{cell} = 1/27 at r_{cell} = 3 mm; at r_{cell} = 8 mm and d_{band}/r_{cell} = 1/3, it is 27943.